nature plants

Article

https://doi.org/10.1038/s41477-024-01865-y

ABA-activated low-nanomolar Ca^{2+}–CPK signalling controls root cap cycle plasticity and stress adaptation

Received: 4 February 2024

Accepted: 28 October 2024

Published online: 22 November 2024

Check for updates

Ziwei Lin[1], Ying Guo[1], Ruiyuan Zhang[1], Yiming Li[1], Yue Wu[2,3], Jen Sheen[2,3] & Kun-hsiang Liu[1,2,3,4]

Abscisic acid (ABA) regulates plant stress adaptation, growth and reproduction. Despite extensive ABA–Ca^{2+} signalling links, imaging ABA-induced increases in Ca^{2+} concentration has been challenging, except in guard cells. Here we visualize ABA-triggered [Ca^{2+}] dynamics in diverse organs and cell types of *Arabidopsis thaliana* using a genetically encoded Ca^{2+} ratiometric sensor with a low-nanomolar Ca^{2+}-binding affinity and a large dynamic range. The subcellular-targeted Ca^{2+} ratiometric sensor reveals time-resolved and unique spatiotemporal Ca^{2+} signatures from the initial plasma-membrane nanodomain, to cytosol, to nuclear oscillation. Via receptors and sucrose-non-fermenting1-related protein kinases (SnRK2.2/2.3/2.6), ABA activates low-nanomolar Ca^{2+} transient and Ca^{2+}-sensor protein kinase (CPK10/30/32) signalling in the root cap cycle from stem cells to cell detachment. Surprisingly, unlike the prevailing NaCl-stimulated micromolar Ca^{2+} spike, salt stress induces a low-nanomolar Ca^{2+} transient through ABA signalling, repressing key transcription factors that dictate cell fate and enzymes that are crucial to root cap maturation and slough. Our findings uncover ABA–Ca^{2+}–CPK signalling that modulates root cap cycle plasticity in adaptation to adverse environments.

Abscisic acid (ABA) is a versatile and central plant hormone that regulates broad developmental processes throughout the plant life cycle including embryogenesis, seed dormancy and germination, organ size, mass and architecture, fertility, and integrative nutrient, metabolic and hormone signalling networks[1–4]. In response to diverse environmental stress conditions, local and systemic synthesis and transport contribute to elevated ABA in various organs and cell types to enhance plant adaptation to and protection from abiotic challenges[2–7]. ABA is perceived by its binding to many functionally redundant or overlapping receptors, PYRABACTIN RESISTANCE1 (PYR1)/PYR1-LIKE (PYL)/REGULATORY COMPONENTS OF ABA RECEPTORS (RCAR)[2]. ABA-bound RCAR/PYR1/PYL complexes with and inhibits the function of clade A Protein Phosphatase 2Cs (PP2Cs). In the absence of ABA, the phosphatase activity of PP2Cs inhibits the kinase activity of sucrose-non-fermenting1-related protein kinases (SnRK2.2/2.3/2.6), which positively regulate the ABA signalling network[2,3].

As a universal cellular messenger, Ca^{2+} mediates diverse signalling events in multiple subcellular compartments of all organisms[8,9]. Temporal patterns in the dynamics of [Ca^{2+}], so-called Ca^{2+} signatures, may appear as rapid spikes, transient or sustained increases above background levels, or oscillating peaks in [Ca^{2+}]. In the cytosol and organelles, Ca^{2+} signatures are often attributed to specific signalling

[1]State Key Laboratory of Crop Stress Biology for Arid Areas and College of Life Sciences, Northwest Agriculture & Forestry University, Yangling, China. [2]Department of Molecular Biology and Centre for Computational and Integrative Biology, Massachusetts General Hospital, Boston, MA, USA. [3]Department of Genetics, Harvard Medical School, Boston, MA, USA. [4]Institute of Future Agriculture, Northwest Agriculture & Forestry University, Yangling, China. e-mail: Sheen@molbio.mgh.harvard.edu; khliu@molbio.mgh.harvard.edu

events in plant development and responses to environmental cues[7–10]. Extensive research supports the idea that Ca^{2+} signalling plays a central role in ABA responses, especially in guard cells[11–14]. For example, multiple Ca^{2+}-sensor protein kinases (CPK3/6/21/23) perceiving endogenous cytosolic $[Ca^{2+}]$ ($[Ca^{2+}]_{cyt}$) oscillations have been shown to phosphorylate and activate S-type anion channels, SLAC1 and SLAH3, to mediate ABA-induced stomatal closure[11–18]. CPK4/11/10/30/32 are implicated in activating gene expression through the phosphorylation and activation of ABA-responsive transcription factors[15,19–21]. Moreover, CPK3/4/6/11 modulates ABA-induced phosphorylation and degradation of guanine nucleotide exchange factor RopGEF1 to facilitate ABA signalling in root hair development and cotyledon growth[22].

Despite molecular, cellular, biochemical and genetic evidence supporting intimate ABA–Ca^{2+} signalling connections in leaf, root and guard cells[11–22], direct imaging of ABA-stimulated $[Ca^{2+}]_{cyt}$ oscillations was feasible only in guard cells[23]. Attempts to visualize and quantify $[Ca^{2+}]$ increases induced by ABA at single-cell resolution in diverse organs and cell types have not been reported, even with the intensity-based Ca^{2+} sensor R-GECO1 which shows a notably higher sensitivity compared to the Forster resonance energy transfer (FRET)-based Ca^{2+} reporter yellow cameleon NES-YC3.6 and YC-nano50 (refs. 23–26).

Genetically encoded Ca^{2+} indicators (GECIs) are indispensable tools for visualizing and quantifying Ca^{2+} signatures in plant and animal cells. The GECIs aequorin, YC3.6, R-GECO1 and GCaMPs have been used to detect changes in local and systemic $[Ca^{2+}]$ induced by a variety of stimuli[9,10,23–32]. Aequorin is a bioluminescence-based Ca^{2+} indicator (with an in vitro dissociation constant (K_d) of 7.2–13 μM for Ca^{2+}) after reconstitution of the holoenzyme with the exogenously applied prosthetic group coelenterazine and has been widely employed at the level of cell populations or entire plants[9,10,30].

Fluorescent-protein-based GECIs bind to Ca^{2+} with nanomolar K_d and are more sensitive to lower intracellular $[Ca^{2+}]$, enhancing the spatiotemporal resolution and sensitivity of Ca^{2+} signalling detection at the single-cell level. Although R-GECO1 (K_d of 482 nM), CGf (K_d of 220 nM) and YC3.6 (K_d of 250 nM) can detect nanomolar levels of $[Ca^{2+}]$, only the ultrasensitive GCaMP6s, exhibiting high affinity with a K_d of 144 nM for Ca^{2+} and a large dynamic range, detected clear nitrate-induced Ca^{2+} signatures in plant leaf and root cells[10,27–30]. To directly visualize and quantify the elusive Ca^{2+} signatures induced by ABA in various plant organs and cell types, we developed reliable and versatile GECI tools that enable the exploration of new ABA–Ca^{2+} signalling mechanisms and the discovery of new ABA functions in plant development and stress adaptation.

Results

Single-cell visualization of ABA-triggered $[Ca^{2+}]$ dynamics

We postulated that an ultrasensitive GECI might reliably detect ABA-induced Ca^{2+} signals in various plant cell types. To support this hypothesis, we performed time-lapse recordings of ABA responses in the roots of transgenic GCaMP6s plants. ABA triggered a rapid Ca^{2+} transient with dual peaks at 100–200 s in the root tip region never previously observed, which were distinct from ABA-activated Ca^{2+} oscillations in guard cells[23,25,26] (Extended Data Fig. 1a). To simplify and improve the quantification of GCaMP6s and maintain its Ca^{2+} sensitivity and high dynamic range, we created a synthetic gene that expressed a single protein with two fluorescent proteins—the green fluorescent GCaMP6s and red fluorescent dTomato—fused by a short SSGS linker (Fig. 1a,b). In this simple Ca^{2+} ratiometric sensor (CRS), the carboxy-terminal dTomato served as a stable internal control insensitive to Ca^{2+} and did not interfere with the Ca^{2+} binding of the amino-terminal GCaMP6s (Fig. 1c). While the Ca^{2+}-induced green fluorescence of CRS was inhibited by EGTA chelation of Ca^{2+}, the red fluorescence of CRS was unaffected (Fig. 1c). Thus, the ratio of Ca^{2+}-sensitive green fluorescence to Ca^{2+}-insensitive red fluorescence of CRS with excitation at 488 nm and 554 nm, respectively, indicates the relative Ca^{2+} signal changes independent of protein expression levels. The K_d of CRS for Ca^{2+} was 165 nM with a Hill coefficient of 3.0 (refs. 27–32) (Fig. 1d and Extended Data Fig. 1h). As a positive control, we first measured $[Ca^{2+}]$ dynamics after nitrate stimulation in mesophyll protoplasts transiently expressing CRS. The ratio of green to red fluorescence showed a similar dynamic Ca^{2+} profile as previously recorded using GCaMP6s[10] (Fig. 1e). Remarkably, we also detected reliable ABA-induced $[Ca^{2+}]$ dynamics with a distinct cytosolic pattern and lower amplitude compared with nitrate-induced dynamics in the transfected mesophyll protoplasts, but not in the mock control without ABA[10] (Fig. 1e–g and Extended Data Fig. 1b).

To enable analyses of ABA-induced Ca^{2+} responses in different plant organs and cell types, we generated CRS transgenic plants with gene expression driven by the constitutive *UBIQUITIN10* (*UBQ10*) promoter. Because ABA-induced Ca^{2+} oscillations were previously observed in guard cells, we first validated the use of CRS in transgenic plants by analysing the ABA-induced Ca^{2+} response in guard cells. Ca^{2+} oscillations in the cytosol of guard cells were observed only after ABA stimulation (Fig. 2a and Extended Data Fig. 2a). We then monitored Ca^{2+} responses in different organs, tissues and cell types, not previously reported. After ABA treatment, the stimulated mesophyll cells initiated a slower Ca^{2+} transient featuring a different shape and kinetics compared with the faster Ca^{2+} transient in the root tip or root differentiation zone, or the more rapid and sharper Ca^{2+} transient in the lateral root primordium (Fig. 2b–e and Extended Data Fig. 2b–d). CRS-based live imaging in plants revealed that ABA could trigger diverse Ca^{2+} signatures distinct from Ca^{2+} oscillations in guard cells and might activate different cellular Ca^{2+} sensors to relay ABA signalling responses in various organs and cell types, as implicated by ABA reporters and next-generation ABACUS biosensors[1–7,11–23,33,34] (Extended Data Fig. 2b–d). Having visualized ABA-triggered $[Ca^{2+}]$ changes in root tips using CRS, we investigated whether other GECIs could similarly detect these changes. We selected the YC3.6 (FRET-based), CGf (GCaMP6f-based) and MatryoshCaMP6s (CaMP6s-based) transgenic lines for monitoring ABA-triggered $[Ca^{2+}]$ changes[24,28,31]. No ABA-triggered $[Ca^{2+}]$ changes were detected in root tips using YC3.6 or CGf (Extended Data Fig. 1d,e). Similar to CRS, ABA triggered a green-fluorescent GCaMP6s signal in MatryoshCaMP6s. However, the LSSmOrange signal, which serves as an internal control, was also triggered by ABA (Extended Data Fig. 1f). The ratio of GCaMP6s to LSSmOrange did not change upon ABA treatment. These results suggest that only GCaMP6s detected clear ABA-induced Ca^{2+} signatures in plant root tips and that CRS serves as a reliable ratiometric calcium sensor.

Spatiotemporal patterns of ABA-triggered Ca^{2+} signalling

Nitrate and ABA appeared to activate different subcellular patterns of $[Ca^{2+}]$ changes and dynamics in mesophyll protoplasts[10] (Fig. 1e–g). Unlike GCaMP6s, which can detect low-nanomolar $[Ca^{2+}]$ changes in both the cytosol and the nucleus[10], CRS was restricted to detecting $[Ca^{2+}]_{cyt}$ (Extended Data Fig. 1g). To overcome the subcellular limit of CRS, we created new versions of CRS localized at the plasma membrane or specific organelles to further characterize Ca^{2+} signatures at high spatiotemporal resolution in different subcellular compartments (Fig. 3a). Transgenic plants expressing CRS fusion proteins showed no obvious growth defect phenotype (Extended Data Fig. 3). We analysed ABA-triggered Ca^{2+} signatures in transgenic plants stably expressing the CRS fusion protein variants targeted to the plasma membrane (CRS-PM), cytosol (CRS) or nucleus (CRS-NLS). As the root tip exhibited prominent ABA-responsive reporter gene expression[33] and Ca^{2+} dynamics (Fig. 2c and Extended Data Fig. 1a,c), we monitored time-resolved ABA-triggered $[Ca^{2+}]$ change patterns in subcellular compartments in the uniform-shaped epidermal cells in the root meristematic zone (Figs. 2c and 3b–f and Extended Data Figs. 2e and 4). When treated with ABA, cells expressing CRS-PM displayed the most rapid elevation of Ca^{2+} signals (<50 s), which appeared to represent the first phase of

https://doi.org/10.1038/s41477-024-01865-y

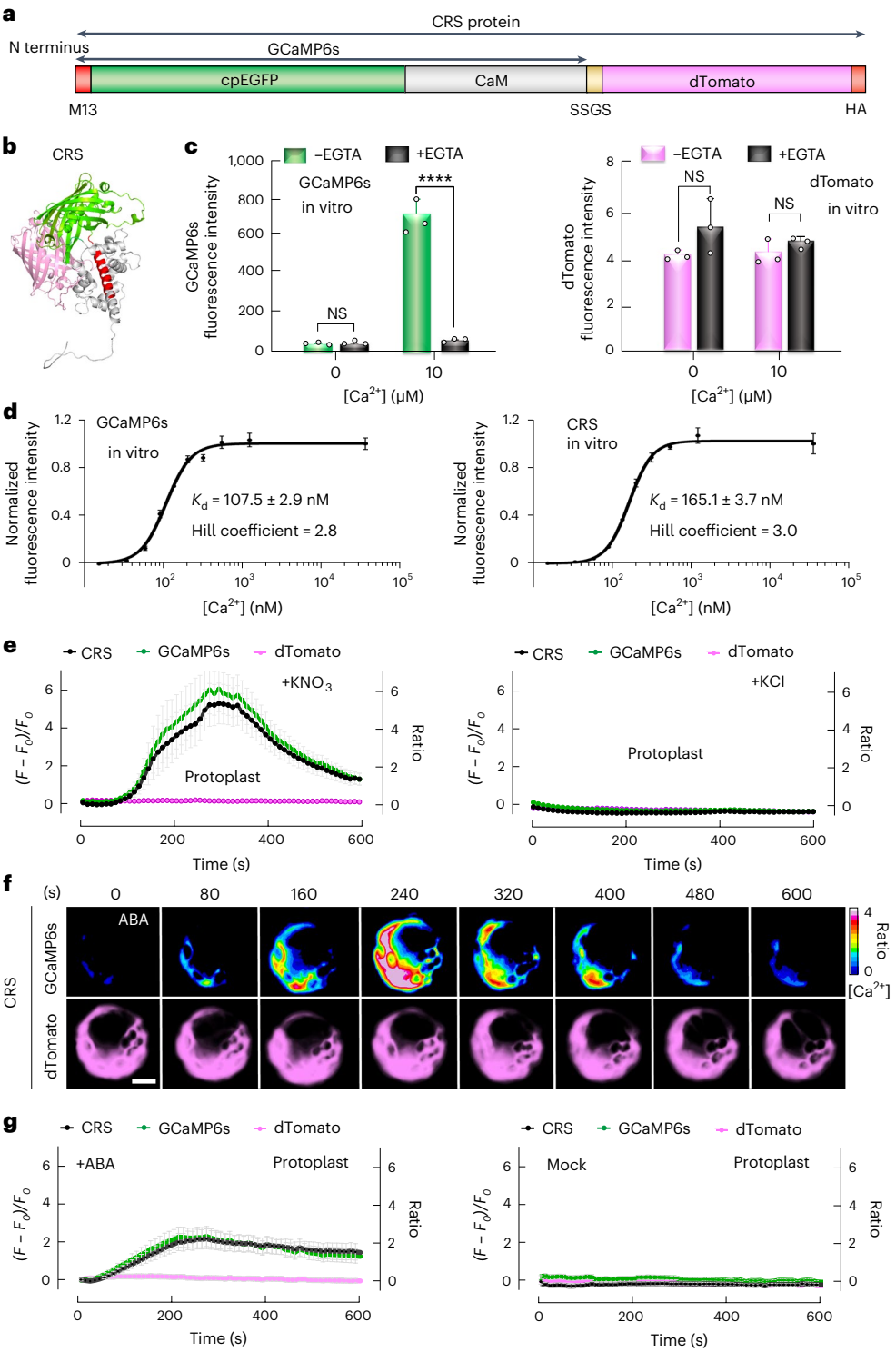

Fig. 1 | An ultrasensitive CRS for detecting ABA-triggered [Ca^{2+}] dynamics. **a**, CRS fusion protein. M13, calmodulin-binding peptide; HA, haemagglutinin. **b**, Structure of CRS predicted by AlphaFold 2. **c**, GCaMP6s fluorescence is activated by calcium in vitro. The bars indicate GCaMP6s (left) or dTomato (right) fluorescence intensity. The error bars denote ±s.e.m. $n = 3$ biological repeats. NS, not significant ($P > 0.05$); ****$P < 0.0001$ (statistical significance was determined by two-tailed non-paired Student's t-tests). **d**, Ca^{2+} titration curves of GCaMP6s and CRS. These results were used to calculate K_d and the Hill coefficient for Ca^{2+}. The error bars denote ±s.e.m. $n = 3$ biological repeats. **e**, Ca^{2+} signalling stimulated by KNO_3 in mesophyll protoplasts expressing CRS. KNO_3 was added at a concentration of 10 mM. $(F - F_0)/F_0$ is the relative fluorescence intensity. 'Ratio' indicates the relative fluorescence ratio of GCaMP6s to dTomato. The error bars denote ±s.e.m. $n = 13$ protoplasts. **f**, Time-lapse images of ABA-triggered Ca^{2+} signalling in mesophyll protoplasts expressing CRS. Scale bar, 10 μm. The images are representative of ten protoplasts. ABA was added at a concentration of 10 μM. **g**, CRS signals stimulated by 10 μM ABA in mesophyll protoplasts expressing CRS. The error bars denote ±s.e.m. $n = 13$ protoplasts. All experiments were conducted in at least three biological repeats, with similar results.

https://doi.org/10.1038/s41477-024-01865-y

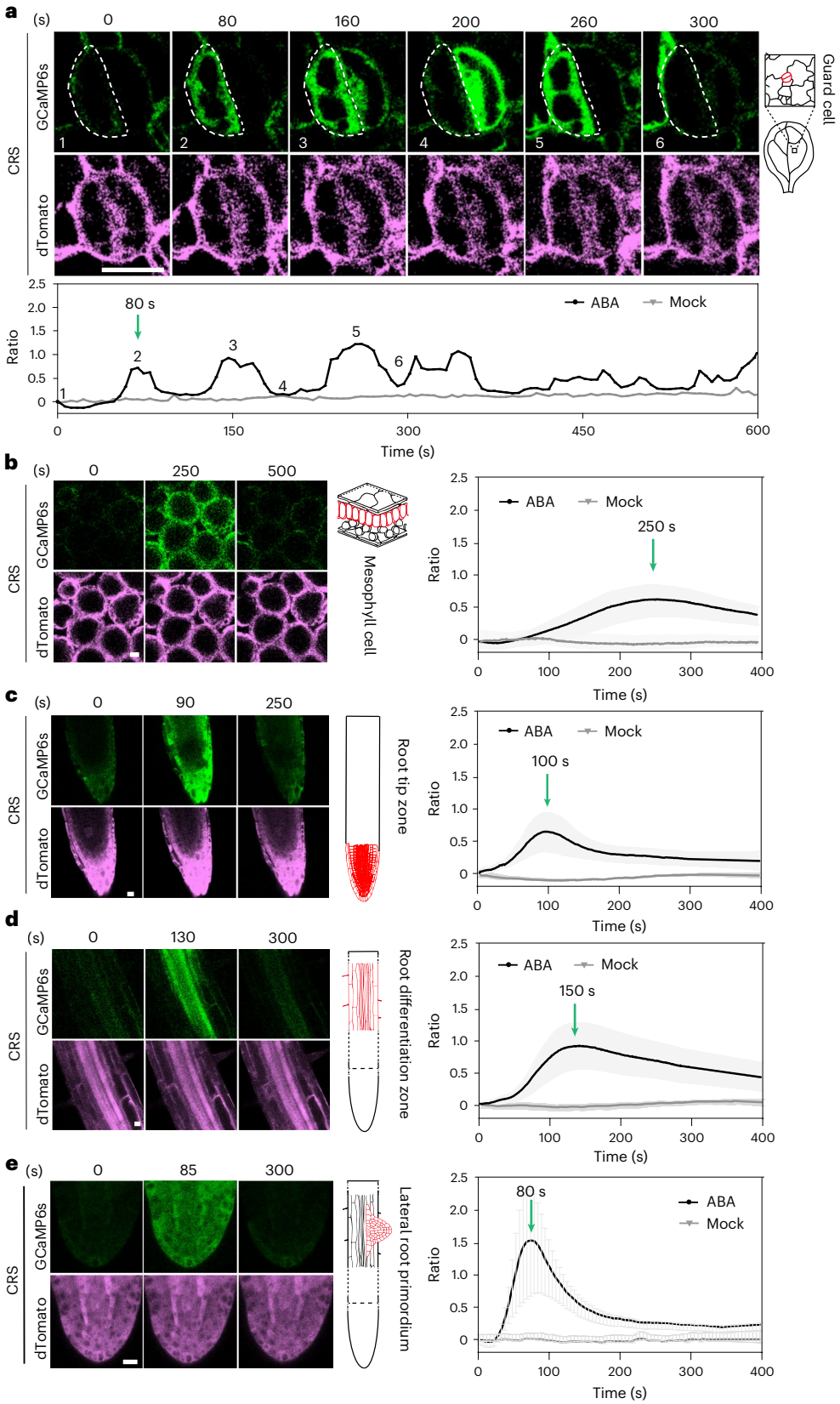

Fig. 2 | ABA triggered different Ca^{2+} dynamics in diverse tissues and cell types. **a**–**e**, Time-lapse images and CRS signals of ABA-stimulated Ca^{2+} signalling. The panels show fluorescence images of GCaMP6s and dTomato and the fluorescence ratio in the guard cells of cotyledons (**a**), mesophyll cells (**b**), the root tip (**c**), the root differentiation zone (**d**) and the lateral root primordium (**e**) of 7-day-old transgenic CRS plants. ABA was added at a concentration of 10 μM. The green arrows indicate the peak of the calcium transient. The error bars denote ±s.e.m. The data are from at least three independent experiments (total number of plants or guard cells: ABA, $n = 6$; mock, $n = 6$ (**a**); ABA, $n = 13$; mock, $n = 10$ (**b**); ABA, $n = 11$; mock, $n = 10$ (**c**); ABA, $n = 15$; mock, $n = 10$ (**d**); ABA, $n = 13$; mock, $n = 9$ (**e**)). Scale bars, 10 μm. 'Ratio' indicates the relative fluorescence ratio of GCaMP6s to dTomato. The monitored region is illustrated in the red-lined drawings. All experiments were conducted in at least three biological repeats, with similar results.

https://doi.org/10.1038/s41477-024-01865-y

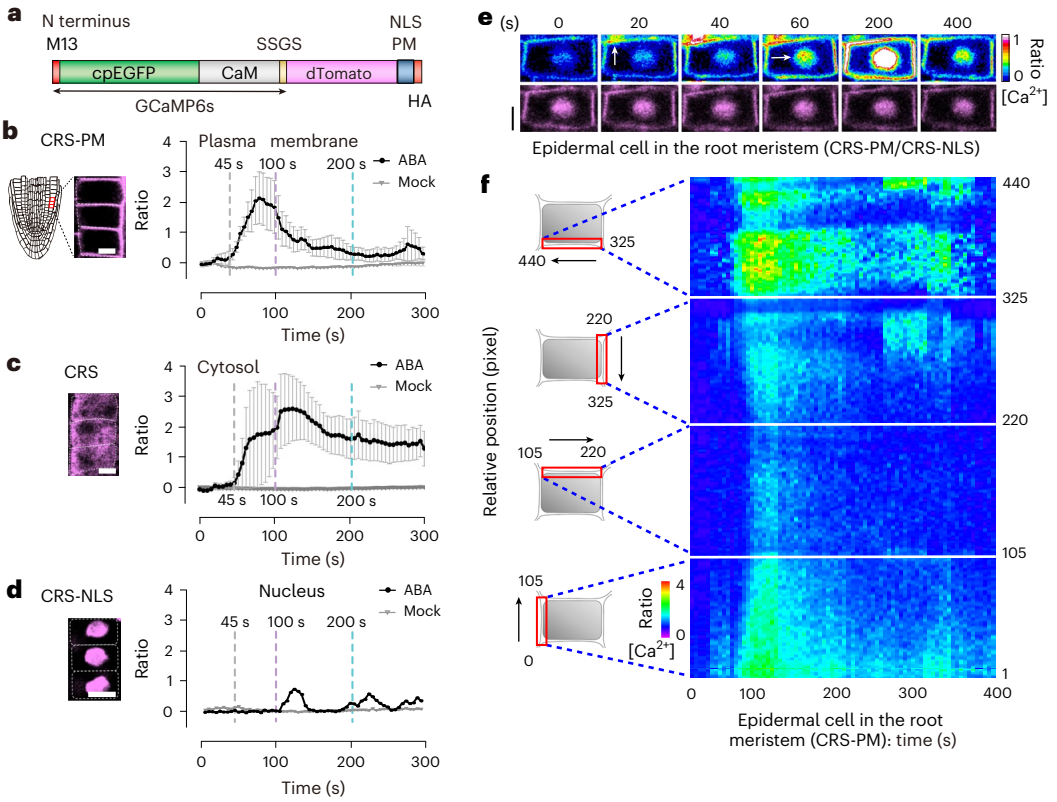

Fig. 3 | ABA-induced dynamic spatiotemporal [Ca^{2+}] changes in the epidermal cells of the primary root tip. a, CRS variants targeted to different subcellular compartments. **b**–**d**, Fluorescence signals of CRS-PM (**b**), CRS (**c**) and CRS-NLS (**d**) stimulated by 10 µM ABA in the epidermal cell of the root meristem zone in 7-day-old transgenic CRS plants. Scale bars, 5 µm. 'Ratio' indicates the relative fluorescence ratio of GCaMP6s to dTomato. The error bars denote ±s.e.m. The data are from at least three independent experiments (total number of plants: ABA, $n = 6$; mock, $n = 6$). The monitored region of epidermal cells in the root meristem zone is illustrated in red-lined cells in **b**. Subcellular localizations of dTomato images from the CRS derivatives are shown. The gray dashed lines mark the onset of cytosolic [Ca^{2+}] elevation at 45 s. The purple dashed lines indicate the second phase of the two-phase cytosolic [Ca^{2+}] increase at 100 s. The blue dashed lines represent a significant decline near the plasma membrane occurring at 200 s. **e**, Time-lapse images of ABA-induced Ca^{2+} transients in epidermal cells in the root meristem zone of 7-day-old plants expressing both CRS-PM and CRS-NLS. The white arrows indicate elevated Ca^{2+} signal. Scale bar, 5 µm. **f**, Kymography analysis of CRS-PM in response to ABA of the epidermal cell in the 7-day-old plant root meristem zone. The red boxes indicate the detection region. The images are representative of three root epidermal cells from three independent experiments. All experiments were conducted in at least three biological repeats, with similar results.

two-phase cytosolic Ca^{2+} increases in timing and amplitude (Extended Data Fig. 1a). The second phase of the elevated cytosolic Ca^{2+} signal was sustained above the initial level of calcium for more than 5 min, whereas a marked decrease occurred near the plasma membrane after 2 min. Unexpectedly, slower (approximately 100 s) but substantial Ca^{2+} oscillation was observed with CRS-NLS (Fig. 3b–d and Extended Data Figs. 2e and 4). Imaging of $[Ca^{2+}]_{cyt}$ changes in single cells expressing CRS variants suggests that the initial Ca^{2+} signal increase due to ABA perception might originate at the discrete nanodomains of the plasma membrane, then spread throughout the plasma membrane and migrate to the cytosol and into the nucleus (Figs. 1f and 3b–d and Extended Data Figs. 2e and 4). These findings are consistent with the detection of ABA receptors and PP2C/ABI1–CPK21 signalling complexes on the plasma membrane nanodomains[35–37].

To directly visualize spatiotemporal ABA–Ca^{2+} signalling processes at the single-cell resolution, we performed time-lapse imaging analysis along the plasma membrane of single CRS-expressing mesophyll cells exhibiting slower ABA-activated [Ca^{2+}] dynamics (Figs. 1f,g and 2b). We found that ABA-triggered Ca^{2+} signal elevations could start from discrete sites and were not evenly distributed along the plasma membrane before migrating into the cytosol (Extended Data Fig. 5a). In the root tip, with faster ABA–Ca^{2+} signalling (Fig. 2c and Extended Data Fig. 1a,c), the CRS seedlings were treated with an extracellular Ca^{2+} chelator, EGTA or BAPTA, or a non-selective Ca^{2+} channel blocker, $GdCl_3$, and the ABA-induced cytosolic Ca^{2+} transient was abolished (Extended Data Fig. 5b). To demonstrate that the ABA-triggered Ca^{2+} signal was first initiated near the plasma membrane[10], we generated a transgenic line harbouring dual CRS-PM and CRS-NLS sensors (CRS-PM/CRS-NLS). When CRS-PM/CRS-NLS seedlings were treated with ABA, Ca^{2+} signals appeared first near the plasma membrane at 10–20 s and then in the nucleus at 50 s in the single epidermal cells of the primary root meristem (Fig. 3e). We further conducted a higher-resolution kymography analysis of CRS-PM in response to ABA by dividing the perimeter of a single root epidermal cell into 440 adjacent regions (Fig. 3f and Extended Data Fig. 6). Combining live imaging analyses in single leaf and root cells with CRS variants provided strong evidence that the elevated Ca^{2+} that originated along the plasma membrane in response to ABA was not homogeneously distributed. CRS enabled ultrasensitive detection of low-nanomolar Ca^{2+} signatures in ABA and nitrate signalling with distinct extracellular and intracellular Ca^{2+} sources and dynamics[10].

Calibration of CRS for quantifying intracellular [Ca^{2+}]

To quantify the precise in vivo low-nanomolar $[Ca^{2+}]_{cyt}$ in response to ABA, we recorded [Ca^{2+}] changes in the root tip of CRS transgenic plants in response to ABA using two references generated by a 1 mM extracellular ATP (eATP)-activated micromolar increase in [Ca^{2+}] and Ca^{2+} chelators to deplete free Ca^{2+} in the root tip cells[24–26] (Fig. 4a).

https://doi.org/10.1038/s41477-024-01865-y

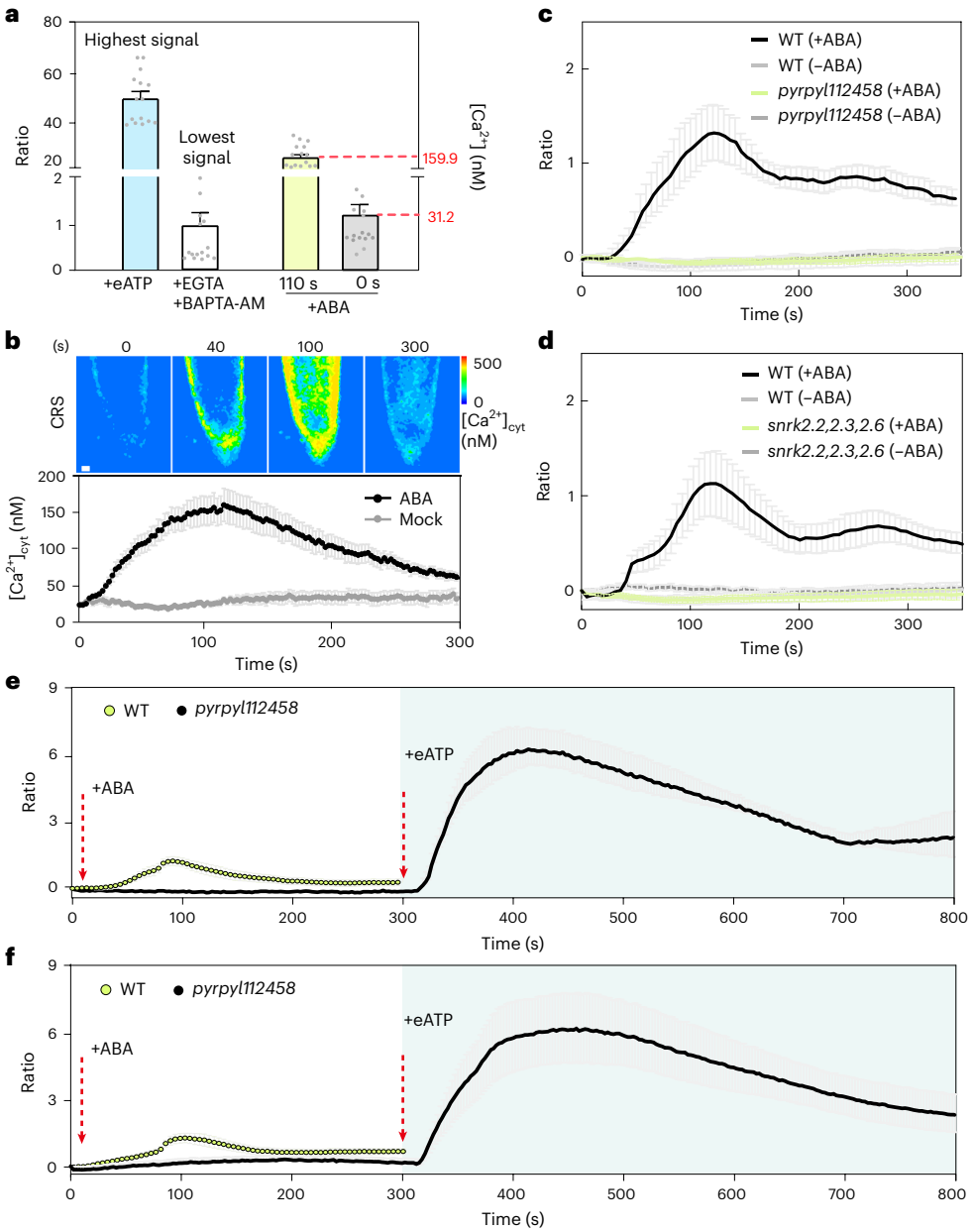

Fig. 4 | ABA-induced low-nanomolar [Ca^{2+}] increases via ABA receptors and SnRK2.2/2.3/2.6. a, Range of ABA-induced changes in [Ca^{2+}]$_{cyt}$. The highest [Ca^{2+}] represents the maximum peak of 10 µM ABA induction (110 s) or 1 mM eATP-induced [Ca^{2+}] in the root tip. The lowest [Ca^{2+}] represents the minimum ABA (0 s) or BAPTA-AM- and EGTA-treated [Ca^{2+}] in the root tip. The error bars denote ±s.e.m. The data are from at least three independent experiments (total number of plants: eATP/EGTA and BAPTA-AM, $n = 15$; ABA, $n = 15$). 'Ratio' indicates the relative fluorescence ratio of GCaMP6s to dTomato. **b**, Time-lapse images and fluoresence signals of ABA-stimulated [Ca^{2+}] changes in the root tip of 7-day-old transgenic CRS plants. The error bars denote ±s.e.m. The data are from at least three independent experiments (total number of plants: ABA, $n = 13$; mock, $n = 10$). Scale bar, 10 µm. **c**,**d**, [Ca^{2+}] transients in 7-day-old *pyrpyl112458–CRS* (**c**) and *snrk2.2,2.3,2.6–CRS* (**d**) root tip cells stimulated by ABA. The error bars denote ±s.e.m. The data are from at least three independent experiments (total number of plants: WT (+ABA), $n = 7$; WT (−ABA), $n = 7$; *pypyrpyl112458* (+ABA), $n = 7$; *pypyrpyl112458* (−ABA), $n = 7$; *snrk2.2,2.3,2.6* (+ABA), $n = 7$; *snrk2.2,2.3,2.6* (−ABA), $n = 7$). **e**,**f**, [Ca^{2+}] transients in 7-day-old *Arabidopsis* root tip cells. WT plants were treated with 10 µM ABA as a control. *pyrpyl112458–CRS* (**e**) and *snrk2.2,2.3,2.6–CRS* (**f**) plants were treated with 10 µM ABA for 5 min and then with 1 mM eATP. The green lines indicate the WT; the black lines indicate the mutants. The error bars denote ±s.e.m. The data are from at least three independent experiments (total number of plants: WT, $n = 7$; *pypyrpyl112458*, $n = 7$; *snrk2.2,2.3,2.6*, $n = 7$). All experiments were conducted in at least three biological repeats, with similar results.

To calibrate and calculate the Ca^{2+} concentration of CRS in the root tip cells, we first treated CRS seedlings with 1 mM eATP to saturate cellular Ca^{2+} and obtain the maximum fluorescence intensity and ratio. We then incubated the same plants in EGTA and BAPTA-AM to acquire the minimum fluorescence intensity and ratio. Treatment with the membrane-permeable detergent digitonin[38] also saturated cellular Ca^{2+}, yielding a similar range of maximum-to-minimum fluorescence intensity ratios in CRS-expressing root tips (Extended Data Fig. 7). Given that the in vitro K_d of CRS for Ca^{2+} is 165 nM with a Hill coefficient of 3.0, we calculated the intracellular [Ca^{2+}] activated by ABA in the root tips (Fig. 4a,b). ABA increased [Ca^{2+}]$_{cyt}$ to approximately 159.9 nM in the root tip cells expressing CRS. Furthermore, CRS-PM and CRS-NLS displayed similar maximum-to-minimum fluorescence intensity and ratio ranges (Extended Data Fig. 7).

ABA-triggered low-nanomolar [Ca^{2+}] via receptors and SnRK2s

Despite decades of intensive research[11–26], how ABA activates [Ca^{2+}] increases has remained unknown in most cell types except guard cells[14,23]. *Arabidopsis* PYR1 and PYL1/2/4/5/8 are functionally redundant ABA receptors that regulate ABA inhibition of primary root formation, while SnRK2.2/2.3/2.6 are key activators of ABA signalling[2,3,36,37]. To determine whether ABA-triggered [Ca^{2+}] increases require ABA receptors and SnRK2.2/2.3/2.6, we generated stable transgenic lines expressing CRS in the sextuple *pyrpyl112458* and triple *snrk2.2,2.3,2.6* mutants[36,37]. The ABA-induced [Ca^{2+}] increase was eliminated in the *pyrpyl112458–CRS* and *snrk2.2,2.3,2.6–CRS* mutants (Fig. 4c,d). To show that the abolished [Ca^{2+}] increase was not due to CRS failure, we treated the same seedlings with 1 mM eATP after recording the ABA responses. A striking [Ca^{2+}] rise was induced by eATP in *pyrpyl112458–CRS* and *snrk2.2,2.3,2.6–CRS*, indicating that the ABA-triggered [Ca^{2+}] increase is regulated downstream of ABA receptors and SnRK2.2/2.3/2.6 (Fig. 4e,f).

ABA–Ca^{2+}–CPK signalling delays the root cap cycle

CRS detected conspicuous ABA-triggered Ca^{2+} signalling in the root tip (Figs. 2c and 4 and Extended Data Fig. 1a,c), where the root cap is located. The root cap plays essential functions in stem cell niche protection, gravitropism, thigmotropism, water/nutrient sensing and uptake, root system architecture, and protection from biotic and abiotic stress[39–43]. To explore ABA–Ca^{2+} signalling functions and regulatory mechanisms in the root cap, we examined the effect of ABA on the unique root cap cycle encompassing the differentiation programs of the columella and lateral root cap cells from stem cell regulation, differentiation and maturation, to detachment[39–43] (Fig. 5a). We first defined the periodicity of the root cap cycle by live imaging of the root cap morphology changes at 3-h intervals for 48 h in 5-day-old seedlings using an ECHO Revolve microscope (Fig. 5b). The average cycle period of root cap initiation and sloughing is approximately 30.4 ± 0.5 h (Fig. 5b). ABA treatment delayed the root cap cycle to approximately 34 ± 0.4 h. To further confirm the involvement of ABA in regulating the root cap cycle, we examined ABA regulation in the sextuple ABA receptor mutant *pyrpyl112458* (Fig. 5b). The *pyrpyl112458* mutant was insensitive to ABA treatment in delaying the root cap cycle. Since ABA triggered a maximum $[Ca^{2+}]_{cyt}$ of 159.9 nM in the root tip of the CRS seedlings (Fig. 4a), we looked to previous studies suggesting that CPK10/30/32, with a higher Ca^{2+} sensitivity than other CPK subgroups, may participate in ABA signalling[10,15,18,44].

Recently, a genetically encoded FRET-based reporter, CPKaleon, was developed to visualize CPK conformational activation, allowing for the recording of Ca^{2+} decoding via CPK21 in guard cells[18]. Since subgroup III CPK10, CPK30 and CPK32 share high protein sequence identity[10,20,44], we constructed CPK32aleon and an additional control, CPK2aleon, which has lower Ca^{2+} sensitivity (Extended Data Fig. 8a), to investigate whether CPK32 can sense ABA-triggered [Ca^{2+}] changes in root cells. We first measured the [Ca^{2+}] response in individual CPKaleons by transiently transfecting and expressing each CPKaleon in root cell protoplasts, followed by treatment with 1 mM $CaCl_2$ and digitonin to saturate intracellular [Ca^{2+}]. CPK2aleon and CPK32aleon recorded conformational changes (Extended Data Fig. 8b). We then focused on CPK32aleon and CPK2aleon to monitor ABA-triggered [Ca^{2+}] changes (Extended Data Fig. 8c). CPK32aleon recorded ABA-triggered [Ca^{2+}] changes, whereas CPK2aleon did not in the root protoplasts. Next, to test whether CPK10/30/32 may serve as the Ca^{2+} sensors to decode ABA–Ca^{2+} signalling in modulating the root cap cycle, we assessed the ABA response in the chemical-inducible triple *icpk* mutant[10] (Fig. 5c). In wild-type (WT) and *icpk* seedlings pretreated with 1-isopropyl-3-(3-methylbenzyl)-1*H*-pyrazolo[3,4-d] pyrimidin-4-amine (3MBiP) induction[10], the average period of the root cap cycle was similar to that in the WT at approximately 31.5 ± 0.7 h. ABA treatment delayed the root cap cycle to 37.5 ± 0.7 h, but this was reduced to approximately 34.3 ± 0.4 h in *icpk* (Fig. 5c).

To elucidate the molecular function of ABA in regulating the root cap cycle, we investigated the expression of key marker genes involved in regulating the differentiation processes. The transcription factor FEZ controls the columella stem cells and the epidermal/lateral root cap stem cells responsible for the initiation of the root cap. The transcription factor SOMBRERO (SMB) promotes root cap differentiation, whereas BEARSKIN 2 (BRN2) is a central transcription factor for the maturation and detachment processes that activates target genes encoding enzymes involved in cell wall degradation (for example, CELLULASE 5 (CEL5), PECTINESTERASE (PE11) and XYLOGLUCAN ENDOTRANSGLUCOSYLASE 5 (XTH5)) and programmed cell death (including RIBONUCLEASE 3 (RNS3) and METACASPASE 9 (MC9))[39–43] (Fig. 5a). Real-time quantitative polymerase chain reaction (PCR) (RT–qPCR) analysis was performed on RNA isolated from the root tips of WT plants and *pyrpyl112458* mutants with or without ABA. The results revealed that ABA activated a typical marker gene, *KIN1* (refs. 14,21), but repressed *FEZ*, *SMB*, *BRN2*, *CEL5*, *XTH5*, *PE11*, *RNS3* and *MC9* expression (Fig. 5d and Extended Data Fig. 9a). The ABA repression of these genes was abolished in the *pyrpyl112458* mutant (Fig. 5d and Extended Data Fig. 9a). Furthermore, to test whether ABA repression of these genes depended on calcium signalling, we pretreated seedlings with or without the membrane-permeable calcium chelator EGTA-AM. ABA repression of *FEZ*, *SMB*, *BRN2*, *CEL5*, *XTH5*, *PE11*, *RNS3* and *MC9* was considerably reduced in EGTA-AM-treated seedlings (Fig. 5e and Extended Data Fig. 9b). Similarly, ABA repression of *SMB*, *BRN2*, *CEL5*, *PE11*, *RNS3* and *MC9* was markedly reduced in the *icpk* mutant. ABA repression of *FEZ*, *CEL5* and *XTH5* required ABA receptors but was partially Ca^{2+}–CPK10/30/32 independent (Fig. 5f and Extended Data Fig. 9c). These data further support the hypothesis that ABA–Ca^{2+}–CPK signalling is involved in regulating the root cap cycle by suppressing the expression of key genes in the developmental program of the entire root cap cycle. Our data indicate that ABA perception and signalling are important for triggering [Ca^{2+}] transients, which repress key genes involved in this cycle. ABA–SnRK2-dependent but Ca^{2+}–CPK-independent signalling may also contribute to the regulation of the root cap cycle.

Salt–ABA–Ca^{2+} signalling modulates the root cap cycle

Current knowledge supports the idea that high salt stress triggers a transient and strong [Ca^{2+}] increase and the classical salt-overly-sensitive (SOS) signalling pathway mediated by the Ca^{2+} sensor SOS3 (CBL4), the protein kinase SOS2 (CIPK24) and the Na^+/H^+ antiporter SOS1 in roots[28,45,46]. However, little is known about salt stress effects on root cap cells. In CRS transgenic plants, we confirmed that 200 mM NaCl activated a sharp 50-s cytosolic Ca^{2+} spike in the root elongation zone (Fig. 6a). Unexpectedly, in contrast to the usual NaCl-activated micromolar [Ca^{2+}] spike, salt stress activated a low-nanomolar [Ca^{2+}] transient, kept the rising [Ca^{2+}] above the initial concentration in root cap cells (Fig. 6b) and substantially delayed the root cap cycle (Fig. 6c). This salt-induced [Ca^{2+}] increase was largely dependent on ABA signalling, as it was strongly reduced in the *pyrpyl112458–CRS* and *snrk2.2,2.3,2.6–CRS* mutants (Fig. 6b). We further demonstrated that salt stress induces ABA accumulation in root cap cells by treating transgenic plants expressing the FRET-based ABA sensor nlsABACUS2-400n with 200 mM NaCl for 30 min (Extended Data Fig. 10a). Our results suggest the involvement of two salt signalling pathways, ABA-dependent and ABA-independent, in orchestrating the salt-stress-induced repression of the root cap cycle. Upon treatment with 200 mM NaCl for 24 h, seedling root tip growth was strongly inhibited, and the root cells turned dark (Extended Data Fig. 10b). To assess the impact of salt stress on the regulation of the root cap cycle, we established a long-term observation method to investigate salt-stress-induced phenotypes. Five-day-old seedlings were treated with 50 mM NaCl, and the differentiation, maturation and detachment of the root cap were monitored under a microscope every 3 h for 60 h. The average period of the root cap cycle from initiation to

https://doi.org/10.1038/s41477-024-01865-y

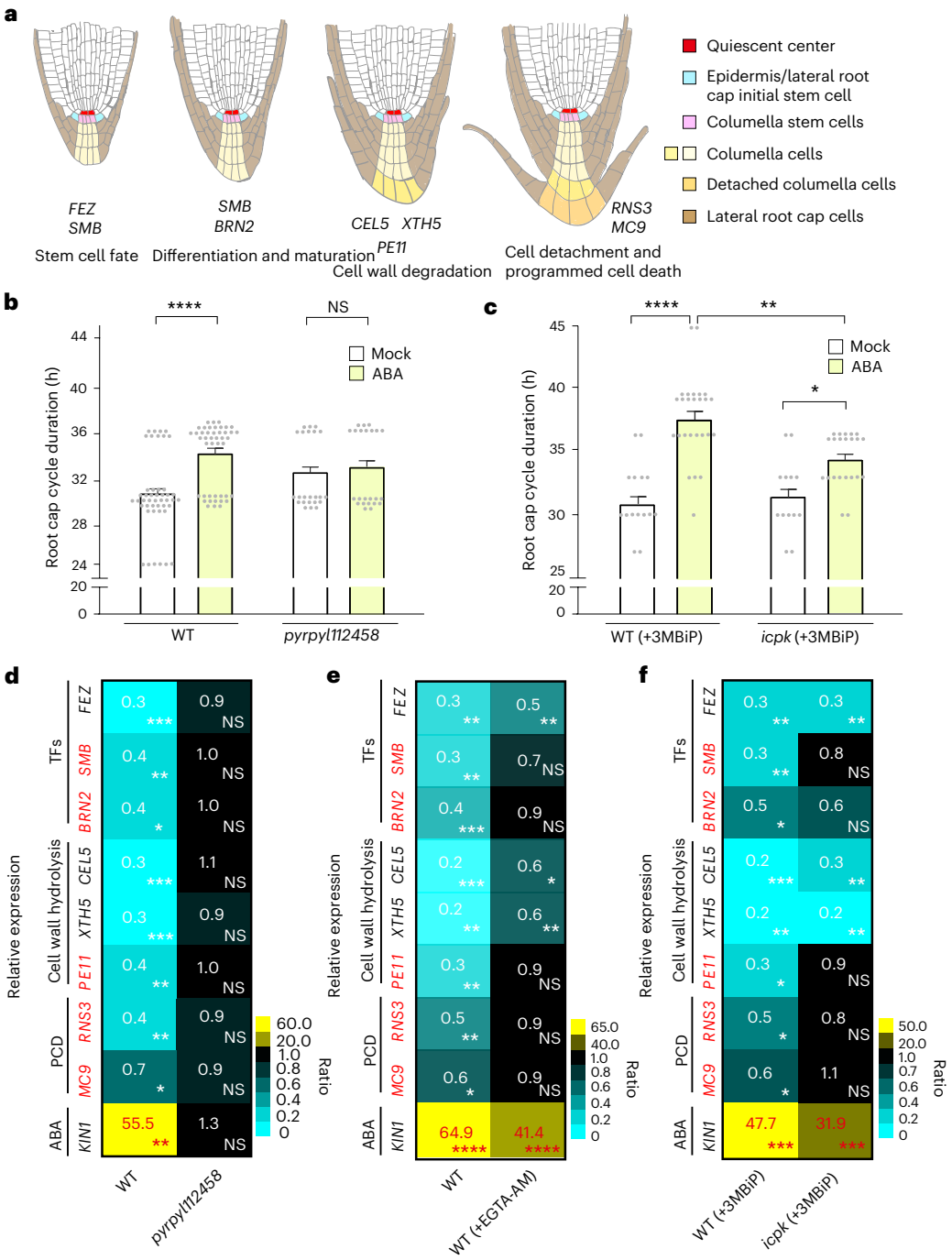

Fig. 5 | ABA delays the root cap cycle and represses genes essential to the root cap cycle. a, Root-cap-formation-related gene functions involved in regulating the root cap cycle. **b**,**c**, Root cap cycle in response to 10 μM ABA treatment in 5-day-old WT, *pyrpyl112458* (**b**) and *icpk* (**c**) plants. To compare the WT and *icpk*, WT or *icpk* plants were pretreated with 0.2 μM 3MBiP for 15 min in the medium. The root cap cycle of 5-day-old WT and *pyrpyl112458* (**b**) or *icpk* (**c**) root tips was monitored under a stereo microscope every 3 h for 48 h. The error bars denote ±s.e.m. The data are from at least three independent experiments (total number of plants: WT mock, $n = 45$; WT ABA, $n = 44$; *pypyrpyl112458* mock, $n = 23$; *pypyrpyl112458* ABA, $n = 23$; WT (+3MBiP) mock, $n = 15$; WT (+3MBiP) ABA, $n = 24$; *icpk* (+3MBiP) mock, $n = 14$; *icpk* (+3MBiP) ABA, $n = 22$). NS, $P > 0.05$; $^{*}P < 0.05$; $^{**}P < 0.01$; $^{****}P < 0.0001$ (statistical significance was determined by two-way analysis of variance with Tukey's multiple comparisons test). **d**–**f**, Heat maps and ratios of RT–qPCR analysis of genes central to the root cap differentiation program in 5-day-old WT and *pyrpyl112458* (**d**) or *icpk* (**f**) root tips in response to ABA treatment, and 5-day-old WT root tips (**e**) with or without 100 μM EGTA-AM pretreatment for 30 min in response to ABA. NS, $P > 0.05$; $^{*}P < 0.05$; $^{**}P < 0.01$; $^{***}P < 0.001$; $^{****}P < 0.0001$ (statistical significance was determined by two-tailed non-paired Student's *t*-tests). TFs, transcription factors; PCD, programmed cell death. 'ABA' denotes an ABA-activated gene. 'Ratio' represents the fold change of genes under ABA treatment compared with the control condition. The genes marked in red are regulated through the ABA–SnRK2–Ca^{2+}–CPK signalling pathway. All experiments were conducted in at least three biological repeats, with similar results.

https://doi.org/10.1038/s41477-024-01865-y

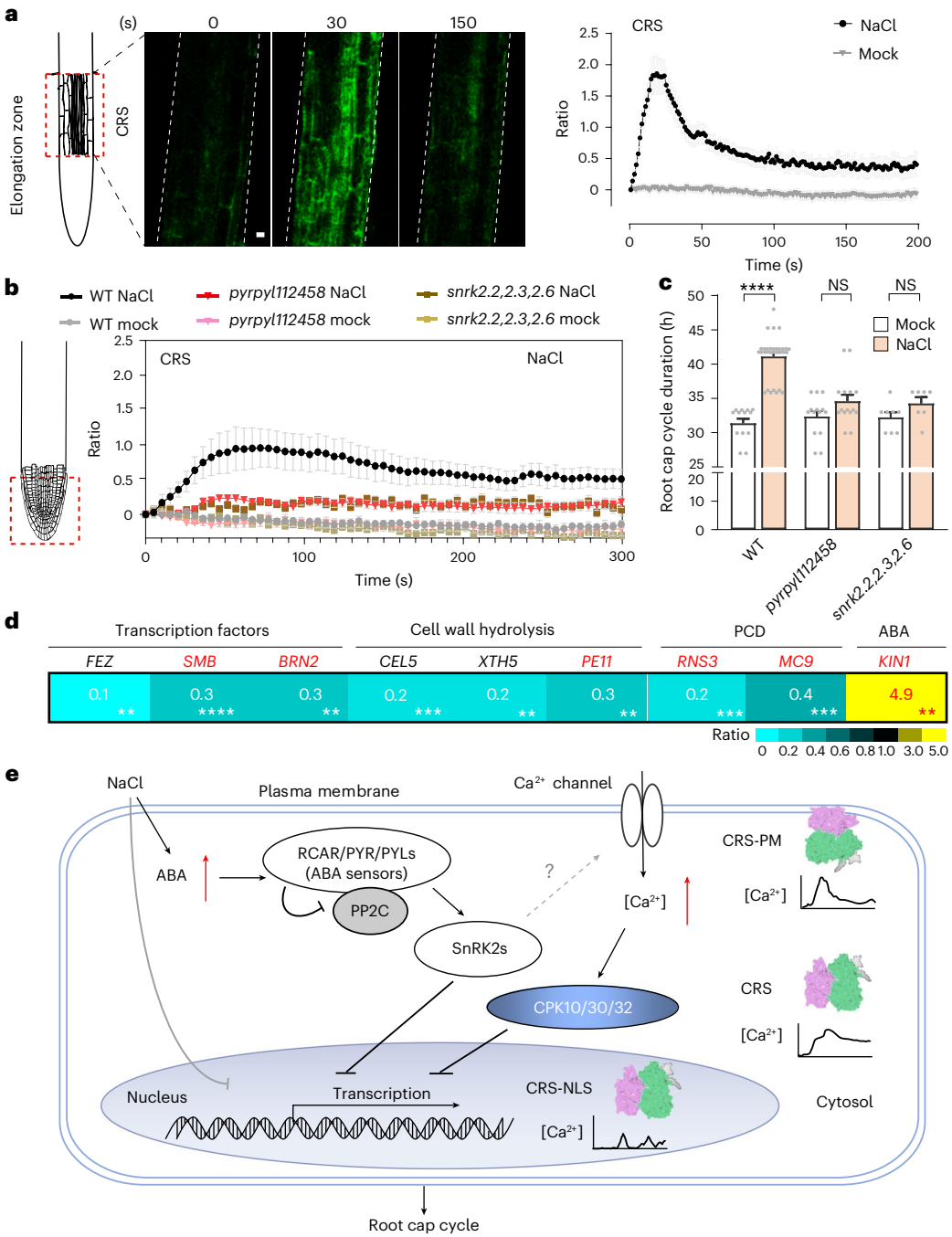

Fig. 6 | Salt stress triggers [Ca^{2+}] transients in the root tip and inhibits the root cap cycle. a, Salt stress induces a rapid [Ca^{2+}] spike in the root elongation zone. Time-lapse images and fluorescence signals of NaCl-stimulated Ca^{2+} signalling in the 7-day-old plant root elongation zone are shown. NaCl was added at a concentration of 200 mM. The error bars denote ±s.e.m. $n = 20$ plants. Scale bar, 10 µm. 'Ratio' indicates the relative fluorescence ratio of GCaMP6s to dTomato. The red dashed line indicates the detection area in the root. **b**, [Ca^{2+}] transients in 7-day-old WT, *pyrpyl112458–CRS* and *snrk2.2,2.3,2.6–CRS* plant root tip cells stimulated by 200 mM NaCl. The error bars denote ±s.e.m. $n = 7$ plants. **c**, The length of the root cap cycle in response to 50 mM NaCl treatment of 5-day-old WT, *pyrpyl112458* and *snrk2.2/2.3/2.6* plants. The error bars denote ±s.e.m. The data are from at least three independent experiments (total number of plants: WT mock, $n = 13$; WT NaCl, $n = 31$; *pypyrpyl112458* mock, $n = 14$; *pypyrpyl112458* NaCl, $n = 15$; *snrk2.2,2.3,2.6* mock, $n = 8$; *snrk2.2,2.3,2.6* NaCl, $n = 7$). NS, $P > 0.05$; $^{****}P < 0.0001$ (statistical significance was determined by two-way analysis of variance with Tukey's multiple comparisons test). **d**, Heat map and ratio of RT–qPCR analysis of genes central to the root cap differentiation program in 5-day-old WT root tip cells in response to 200 mM NaCl or mock treatment. $^{**}P < 0.01$; $^{***}P < 0.001$; $^{****}P < 0.0001$ (statistical significance was determined by two-tailed non-paired Student's *t*-tests). 'ABA' indicates an ABA-activated gene. 'Ratio' represents the fold change of genes under ABA treatment compared with the control condition. The genes marked in red are regulated through the ABA–SnRK2–Ca^{2+}–CPK signalling pathway. All experiments were conducted in at least three biological repeats, with similar results. **e**, A proposed model for the regulation of the root cap cycle through calcium signalling in response to NaCl stress and ABA treatment. Distinct low-nanomolar [Ca^{2+}] dynamics triggered by ABA in different subcellular compartments are revealed by CRS-PM, CRS and CRS-NLS. ABA-triggered [Ca^{2+}] transients are downstream of ABA receptors (RCAR/PYR/PYL) and downstream regulators (SnRK2s). ABA and calcium signalling are important for regulating gene expression and the root cap cycle. Salt stress induces ABA accumulation and [Ca^{2+}] increases in root tip cells, and represses root-cap-cycle-related gene expression through or independent of the downstream effectors CPK10/30/32.

shedding was delayed from 31.4 ± 0.7 h (in mock treatment) to approximately 41.1 ± 0.6 h with NaCl treatment (Fig. 6c). The root cap cycle was not notably delayed in the *pyrpyl112458* and *snrk2.2,2.3,2.6* mutants with 50 mM NaCl treatment (Fig. 6c). Additionally, RT–qPCR analysis was performed with RNA isolated from the root tip of WT seedlings with or without 200 mM NaCl treatment. Salt stress activated the expression of *KIN1*, a salt-stress- and ABA-responsive gene[21], while it repressed *FEZ*, *SMB*, *BRN2*, *PE11*, *RNS3*, *MC9*, *XTH5* and *CEL5* expression (Fig. 6d and Extended Data Fig. 9d), resembling ABA repression (Fig. 5d–f and Extended Data Fig. 8). The data presented here connect salt stress, ABA and Ca^{2+} signalling in controlling the root cap cycle (Fig. 6e).

Discussion

Despite decades of research, the full physiological functions of ABA as a versatile plant hormone and its wide-ranging signalling mechanisms remain incompletely understood[1–7,11–23,33,34]. The molecular links of ABA–Ca^{2+} signalling are especially enigmatic in most plant organs and cell types[11–26]. The simple design and easy application and modification of CRS offer several advantages over other prevalent Ca^{2+} biosensors based on aequorin, YC3.6, YCnano50, R-GECO1, CGf, CamelliA and MatryoshCaMP6s[23–32] for new investigations of ABA–Ca^{2+} signalling in plants. CRS exhibits high sensitivity, a large dynamic range and a fast response. Single-cell ratiometric imaging by the stable single fusion of GCaMP6s[10,27–30] and dTomato for dual fluorescence displays low phototoxicity suitable for tagged protein monitoring (Extended Data Fig. 1h). CRS and its variants localize in different subcellular compartments and organelles, representing ultrasensitive and versatile Ca^{2+} imaging tools that enable real-time quantitative and comparative detection at high spatiotemporal resolutions without disturbing plant growth and development[25,29] (Extended Data Fig. 3). With CRS, we have demonstrated that ABA triggers different and previously unknown cytosolic Ca^{2+} signatures in shoot and root cells distinct from the Ca^{2+} oscillation in guard cells[23]. Despite a high correlation between ABA and abiotic stress, ABA-induced cytosolic Ca^{2+} signals are markedly slower but more sustained with lower amplitude compared with the rapid, strong and very transient and sharp Ca^{2+} spikes characteristic of cold, salt and osmotic stress responses[8,9,28,30]. Direct visualization and recording of distinct [Ca^{2+}] dynamics with CRS and its subcellular derivatives could be broadly applied in investigating physiological responses to other phytohormone, nutrient, chemical, physical or peptide signals that may elicit sensitive and specific Ca^{2+} responses in localized subcellular compartments and nanodomains with previously unrecognized physiological roles in plants.

Chelation of apoplast Ca^{2+} by EGTA and BAPTA blocked ABA-induced [Ca^{2+}] changes, suggesting an extracellular source of Ca^{2+} in root cells in response to ABA. Distinct patterns of ABA-activated [Ca^{2+}] dynamics, initiating from the plasma membrane, migrating to the cytoplasm and triggering nuclear oscillation, further support this hypothesis. ABA-induced Ca^{2+} signalling appears to initiate at nanodomains of the plasma membrane in leaf mesophyll and root meristem epidermal cells, consistent with the detection of ABA receptors and signalling components[35,37]. Rapid Ca^{2+} propagation around the plasma membrane may reflect positive feedback in Ca^{2+} signalling associated with recruiting more ABA receptor complexes[35,37] and amplified Ca^{2+} channel activation[14]. Future research may reveal whether specific nanodomains are enriched with Ca^{2+}-permeable channels and/or ABA signalling components and how [Ca^{2+}] dynamics are decoded and coordinated for cell-type-specific and organelle- or subcellular-specific ABA responses.

FRET-based ABA indicators detect ABA accumulation in the root[34] (Extended Data Fig. 10a). However, R-GECO1, YC3.6 and CGf, Ca^{2+} indicators failed to detect ABA-triggered Ca^{2+} signals in roots[25,26] (Extended Data Fig. 1d,e). Our results with CRS revealed that ABA triggered low-nanomolar [Ca^{2+}] increases up to approximately 159.9 nM calibrated in the root tip. Although MatryoshCaMP6s also detected this Ca^{2+} change, its internal control increased upon ABA treatment, making it unsuitable for ratiometric quantification of ABA–Ca^{2+} signalling. Therefore, only ultrasensitive Ca^{2+} indicators such as GCaMP6s and CRS can overcome the limitations of R-GECO1, CGf and YC3.6 (refs. 23–26,31,32) (Extended Data Fig. 1d,e,h). We also found that CPK10/30/32 are low-nanomolar Ca^{2+} sensors contributing to the signalling decoding specificity responsible for ABA and nitrate[10,44] responses in the root cap and perhaps also in other organs and cell types and in different subcellular compartments. In guard cells, CPK3/6/21/23 (responsible for ABA signalling and relaying the unique cytosolic Ca^{2+} oscillation) appeared to require higher [Ca^{2+}] for full activation[15–18,44]. The differential activation of different CPKs as natural plant Ca^{2+} sensors in different cell types in response to ABA may explain the detection of ABA-activated cytosolic Ca^{2+} oscillation by FRET-based YC2.1 and YC3.6 with lower dynamic ranges and Ca^{2+} affinities than GCaMP6s and CRS variants[15–18,44].

The application of CRS in *Arabidopsis* plants led to our discovery that ABA triggers [Ca^{2+}] dynamics in the root tip and delays the root cap cycle via PYR/PYL–SnRK2–CPK10/30/32 signalling. These findings suggest that ABA represses the root cap cycle as a stress adaptation and protection mechanism. As most research has focused on ABA-activated genes[1–7,19–21], our study reveals the often-overlooked functional importance of ABA-repressed genes that encode cell-fate-regulating transcription factors and enzymes involved in cell-wall degradation and programmed cell death, which contribute to modulating root cap cycle plasticity. Further exploration of ABA-repressed genes may uncover novel ABA functions and regulatory mechanisms in plant development and reproduction[1–7,33,34].

The root cap plays crucial roles in protecting the stem cell niche and regulating the directional growth of roots by sensing environmental stimuli and triggering various tropisms. Rapid and precise turnover of the root cap, from cell division to sloughing, is essential for the plant to adapt to varying environmental conditions[39]. Salt stress strongly inhibits root elongation and alters root growth direction, with an increase in calcium levels being an early response to salt stress[45]. This dynamic turnover process enables the root cap to effectively manage and respond to environmental challenges, ensuring protection of the stem cell niche and optimal root growth and development. In CRS transgenic plants, we confirmed that NaCl activated the prevailing [Ca^{2+}] spike in the root elongation zone. However, in contrast to the typical NaCl-activated micromolar [Ca^{2+}] spike, our study with CRS revealed that salt stress activates a low-nanomolar [Ca^{2+}] transient via ABA, leading to an increase in $[Ca^{2+}]_{cyt}$ specifically within root cap cells, which concurrently delayed the root cap cycle. It has been reported that it took 6 h in multiple root zones above the root cap to respond to shoot-derived ABA stimulated by NaCl treatment in *Arabidopsis* seedlings expressing nlsABACUS2 biosensors[34]. However, NaCl appears to stimulate ABA accumulation in the root cap within minutes (Extended Data Fig. 10a). This suggests that ABA–Ca^{2+} signalling in the root cap may involve a distinct local source of ABA. Moreover, salt and ABA signalling target and repress common key transcription factors dictating cell fate and enzymes activating cell-wall degradation and cell death, which are crucial to root cap maturation and slough. Unveiling the precise Ca^{2+} channel, transporter or Ca^{2+}-permeable protein that facilitates ABA-mediated increases in $[Ca^{2+}]_{cyt}$ distinct from the canonical SOS signalling pathway will lead to new insights into plant salt stress signalling.

Ca^{2+} signalling may also interface with many other regulatory mechanisms in the root cap cycle. Exploiting the CRS transgenic line as a research tool holds the potential to address these inquiries through the investigation of Ca^{2+} signalling responses to diverse stimuli. Currently, the signalling mechanisms that converge and control the development of the root cap cycle are poorly understood. Future research will reveal the integrated regulatory network that modulates root cap development via other transcription factors, peptides, hormones and

environmental cues—for instance, how ABA and the WOX5 transcription factor acting in the root quiescent centre synergistically block the differentiation of the root cap stem cells[33,47], and how ABA, auxin and cytokinin signalling crosstalk in columella and lateral root cap cells[33,39,42,47,48]. Intriguingly, nitrate and ABA signalling interact and regulate the root cap cycle by initiating distinct subcellular Ca^{2+} transients but sharing ultrasensitive CPKs and the NLP7 and SMB transcription factors[10,39–42]. It will also be important to determine the downstream signalling mechanisms that interconnect IDL1–HSL2 peptide–receptor kinase and ABA signalling with antagonistic functions in modulating the root cap cycle[43].

Methods

Plasmid constructs and transgenic lines

The 1.3 kb GCaMP6s coding region was amplified by PCR from the *pHBT–GCaMP6s* plasmid[10] using the primers GCaMP6s-F and GCaMP6s-R (Supplementary Table 1). The 0.7 kb dTomato coding region was amplified by PCR from the *pHBT–tdTomato* plasmid[10] using the primers dTomato-F and dTomato-R (Supplementary Table 1). The promoter is available from the Arabidopsis Biological Resource Center (*pHBT–sGFP(S65T)–NOS*, EF090408 CD3-911). A GS linker (AGTTCCGGATCT) fused the two fragments, and they were subcloned into the BamHI and StuI sites of the *pHBT–tdTomato* plasmid using a Gibson Assembly kit (New England Biolabs). The plasmid *pUBQ10–CRS* was generated by replacing the HBT promoter with the *UBQ10* promoter using the primers UBQ10-F and UBQ10-R (Supplementary Table 1).

For nuclear or plasma membrane localization, C-terminal targeting sequences (Supplementary Table 2) were added to the *CRS* construct using designed oligonucleotides with the ATG start codon and restriction sites. PCR amplified products were cloned into the BamHI and StuI sites using Gibson Assembly. The plasma membrane localization sequence was amplified from *Arabidopsis* genomic DNA using the primers listed in Supplementary Table 1. The PCR fragments were cloned into the BamHI and StuI sites of the *CRS* plasmid using the Gibson Assembly method. The different *CRS* constructs were amplified and inserted into the binary vector *pGIIB–p35S–LIC–NOSt*[49], and the *Agrobacterium* (GV3101)-mediated floral-dip method was applied to generate transgenic plants harbouring the *CRS* constructs. The transgenic plants were selected after they had been sprayed with Basta herbicide. To obtain *pyrpyl112458* and *snrk2.2,2.3,2.6* mutants expressing CRS, *pyrpyl112458* and *snrk2.2,2.3,2.6* were crossed with the CRS transgenic line. Homozygous *pyrpyl112458–CRS* and *snrk2.2,2.3,2.6–CRS* were characterized by genotyping. The DNA sequence of *CPKaleons* was synthesized by Sangon Biotech and then cloned into a plant expression vector containing the HBT promoter. The sequences of *CPKaleons* are listed in Supplementary Table 4.

Plant materials and growth conditions

Arabidopsis ecotype Columbia (Col-0) was used as the WT. The *pyrpyl112458* and *snrk2.2,2.3,2.6* seeds were provided by J.-K. Zhu, the CGf transgenic line by J. F. Harper, the YC3.6 transgenic line by A. Miyawaki, nlsABACUS2-400n by A. Jones and MatryoshCaMP6s by the Arabidopsis Biological Resource Center. To monitor ABA-triggered Ca^{2+} changes and the dynamic range of CRS variants, 10–15 transgenic seedlings of CRS, CRS-PM and CRS-NLS were grown in each well of a six-well tissue culture plate (Corning) containing 1 ml of ½ Murashige and Skoog Basal Salt Mixture (MS) medium (Caisson) with 1 g l^{-1} MES and 1% sucrose, at pH 5.8 (½ MS medium). The seedlings were maintained under a 12-h light/12h dark photoperiod at 23 °C for 7 days. Seedlings for comparing ABA-induced Ca^{2+} signal detection in CGf, YC3.6 and MatryoshCaMP6s were grown similarly. To obtain nitrate-free mesophyll protoplasts, 20 plants were grown on a petri dish (150 mm × 15 mm) containing 100 ml of nitrogen-free 1× MS medium (MSP07, Caisson) with 0.1% MES, 1% sucrose, 0.8% phytoagar (PlantMedia) and 2.5 mM ammonium succinate, pH 5.8. The growth conditions were 12 h light/12 h dark at 23 °C for 23–28 days. Leaves were digested in an enzyme solution containing 20 mM MES (pH 5.7), 0.4 M mannitol, 20 mM KCl, 10 mM $CaCl_2$, 1.25% cellulase (Yakult) and 0.3% macerozyme (Yakult) for 3–4 h on a benchtop orbital shaker at ~50 rpm. The cells were filtered through 70 µm strainers and pelleted at 100 *g* for 2 min. The protoplasts were resuspended in 10 ml of W5 solution and then rested on ice for 30 min. After the W5 solution was removed, the protoplasts were resuspended to ~2 × 10^5 cells per ml in MMG[10] solution (4 mM MES at pH 5.7, 0.4 M mannitol and 15 mM $MgCl_2$). For transfection, 1 ml of the cell suspension was mixed with 100 µl (~100 µg) of plasmid DNA and 1.1 ml of PEG[10] solution (40% (w/v) PEG4000 (81240, MilliporeSigma), 0.2 M mannitol and 100 mM $CaCl_2$) in a 10 ml tube for 5 min. The mixture was diluted with W5 solution (2 mM MES at pH 5.7, 154 mM NaCl, 125 mM $CaCl_2$ and 5 mM KCl) and gently mixed to stop the transfection. The protoplasts were pelleted at 100 *g* for 2 min, the supernatant was removed and the cells were resuspended in WI (ref. 10) solution (4 mM MES at pH 5.7, 0.5 M mannitol and 20 mM KCl). The protoplasts were then incubated under constant light at 23 °C for 6–12 h. For shoot development comparison in the WT, CRS, CRS-NLS and CRS-PM, plants were grown in soil (Pindstrup) under constant light (120 µmol m^{-2} s^{-1}) at 23 °C for 21 days. Photos were taken using a digital camera (Canon DOS80D) and processed using Adobe Photoshop (v.29.0). Flowering time was assessed in soil-grown WT, CRS, CRS-NLS and CRS-PM plants under constant light (120 µmol m^{-2} s^{-1}) at 23 °C until flowering. Fresh weight, root length and leaf area were measured in WT, CRS, CRS-NLS and CRS-PM seedlings grown in square petri dishes containing ½ MS solid medium (½ MS medium with 0.8% phytoagar) under constant light at 23 °C for 7 days. Root length and leaf area were quantified using ImageJ 1.53t[50] from photos taken with a digital camera. Flowering time was recorded as days to bolting (stems ~3 mm)[51]. The data were processed with GraphPad Prism (version 8.0 for Windows, GraphPad Software, Boston, MA, USA; www.graphpad.com) and Adobe Photoshop. Root progression was monitored by growing one seedling per well in a 12-well plate with 0.5 ml of ½ MS medium under constant light at 23 °C for 5 days. Gene expression was induced in the WT or *pyrpyl112458* with 10 µM ABA or 0.1% ethanol (mock) for 4 h. WT and *icpk* seedlings were pretreated with 10 µM 3MBiP for 15 min, followed by 4 h of treatment with 10 µM ABA or 0.1% ethanol (mock). For the Ca^{2+} chelation assay, WT seedlings were pretreated with 100 µM EGTA-AM or 0.1% DMSO (mock) in 1 ml of ½ MS medium for 30 min, followed by treatment with 10 µM ABA or 0.1% ethanol (mock) for 4 h. For the salt stress assay, seedlings were treated with 200 mM NaCl or H_2O (mock) in 1 ml of ½ MS medium for 2 h. Root tip protoplasts were obtained from WT seedlings grown in ½ MS solid medium under constant light at 23 °C for 10 days. For protoplasting and transfections, one third of the roots from the root tip were harvested, and the cell walls were removed using the enzyme solution described above for 5–6 h. The cells were filtered sequentially through 70 µm and 40 µm cell strainers and pelleted at 500 *g* for 5 min. The filtered cells were washed with MMG[10] solution and resuspended to approximately 2–3 × 10^6 cells per ml. For each transfection, 50 µl of the cell suspension was mixed with 5 µg of plasmid DNA and 55 µl of PEG[10] solution in a 2 ml centrifuge tube for 10 min. Then, 500 µl of W5 (ref. 10) buffer was slowly added to the tube. The mixture was centrifuged at 500 *g* for 5 min at room temperature using a bench-top centrifuge, and the supernatant was removed. The protoplasts were gently resuspended with 0.25 ml of WI (ref. 10) in each well of a 24-well tissue culture plate and incubated under constant light at 23 °C for 10–12 h. For analysis of salt-stress-induced ABA accumulation in nlsABACUS2-400n, seedlings were grown in six-well plates with 1 ml of ½ MS medium under a 12 h light/dark cycle at 23 °C for 7 days.

CRS-based Ca^{2+} imaging and analysis

CRS-based Ca^{2+} imaging in mesophyll protoplasts was employed as previously described[10]. Briefly, for nitrate-triggered Ca^{2+} changes,

nitrate-free protoplasts (2×10^5) in 1 ml of buffer were transfected with 100 µg of CRS plasmid DNA and incubated in 5 ml of WI buffer for 6 h. KCl or KNO_3 (10 mM) was added for stimulation. For ABA-triggered changes, 1 ml of four-week-old mesophyll protoplasts (2×10^5 per ml) from soil-grown plants were transfected with 100 µg of CRS plasmid and then stimulated with 10 µM ABA. Imaging was performed with Leica AF software using a Leica DM5000B microscope at ×20. The GCaMP6s and dTomato exposure times were 0.5 s and 0.2 s, recorded every 10 s. Fluorescence data were processed using Microsoft Excel, and the images were edited in Adobe Photoshop.

For guard and mesophyll cells, root tips and roots, 10–15 CRS seedlings were grown in a six-well plate with 1 ml of ½ MS medium under 12 h light/12 h dark at 23 °C for 7 days. A chamber slide was prepared with cover slips and invisible tape, embedding seedlings in the medium. Ca^{2+} imaging was analysed with a Leica TCS SP8X DSL confocal microscope. The stimulus buffer (15 µl, ½ MS medium with 40 µM ABA or 0.1% ethanol) was applied, achieving a final ABA concentration of 10 µM. For GCaMP6s and dTomato, excitation was set at 488 nm and 554 nm, with emissions at 497–520 nm and 571–610 nm, respectively. Microscope magnification was ×63 for high-resolution areas (1,024 × 1,024 pixels) and ×20 for root tips (512 × 512 pixels), captured every 0.868 s or 5.12 s. Subcellular localization and Ca^{2+} imaging was processed using Leica software, ImageJ and Adobe Photoshop, with GraphPad Prism used for traces. For Ca^{2+} channel blockers, seedlings were pretreated with 2 mM $GdCl_3$, 20 mM EGTA or 50 µM for 30 min. ABA-induced Ca^{2+} changes in *pyrpyl112458–CRS* and *snrk2.2,2.3,2.6–CRS* mutants were recorded before and after adding 1 mM ATP. NaCl-induced changes were similarly monitored in these mutants and CRS root elongation regions, stimulated by 200 mM NaCl or water (mock).

To assess the dynamic range of CRS variants, 7-day-old transgenic seedlings (CRS, CRS-PM and CRS-NLS) were treated with 1 mM $CaCl_2$ and 100 µM digitonin for 20 min. Fluorescence images of root tips were captured using a Leica M205 FA microscope. The seedlings were then incubated in 20 mM EGTA and 50 µM BAPTA-AM for 15 min, followed by additional imaging. All images were acquired with a ×16 objective lens and 1 s exposure time for both GCaMP6s and dTomato. Intensity data were analysed using Microsoft Excel for Mac 16.89.1 (24091630) and GraphPad Prism.

The signal values of GCaMP6s and dTomato fluorescence intensity were extracted from the indicated regions. The dynamic fluorescence intensity values (ΔF) were calculated as $(F - F_0)/F_0$, where F_0 represents the starting point value. The ratio was calculated as $\Delta(F_{GCaMP6s}/F_{dTomato})$. To generate a Ca^{2+} imaging heat map of CRS-PM in the primary root meristem, fluorescence ratio values along the plasma membrane were cropped and divided into 440 segments. The heat map was generated using ImageJ and GraphPad Prism.

For $[Ca^{2+}]$ calibration in root tip cells, CRS seedlings were treated with 1 mM eATP to saturate cellular Ca^{2+}, providing the maximum fluorescence ratio (R_{max}): $R_{max} = ((F_{GCaMP6s}max - F_0)/F_0)/\Delta F_{dTomato}$. Subsequently, the seedlings were incubated in EGTA and BAPTA-AM to obtain the minimum ratio (R_{min}): $R_{min} = ((F_{GCaMP6s}min - F_0)/F_0)/\Delta F_{dTomato}$. The dynamic fluorescence ratio at each time point was calculated as $R_\Delta = ((F_{GCaMP6smax} - F_0)/F_0)/\Delta F_{dTomato}$ with R_{min} set to 1, and R_{max} and R_Δ normalized relative to R_{min}. Using the Hill equation and an in vitro K_d of 165.1 nM for CRS with a Hill coefficient (h) of 3.0, $[Ca^{2+}]_{cyt}$ was determined as follows:

$$[Ca^{2+}]_{cyt} = K_d \times ((R_\Delta - R_{min})/(R_{max} - R_{min})) /(1 - /((R_\Delta - R_{min})/(R_{max} - R_{min})))^{(1/h)}$$

GCaMP6s-based Ca^{2+} imaging and analysis

For Ca^{2+} imaging in GCaMP6s transgenic root tips, a chamber slide was prepared using two strips of tape along the edges of a 50 mm × 24 mm cover slip coated with 45 µl of ½ MS medium. A 7-day-old seedling was embedded in the medium, with a thin cotton layer placed over the cotyledon, and a 24 mm × 24 mm cover slip was secured on top. The seedling recovered for 10–20 min before imaging with a Leica TCS SP8X DLS confocal microscope. Then, 15 µl of buffer (½ MS medium with 40 µM ABA or 0.1% ethanol) was applied along the cover slip edge, resulting in a final ABA concentration of 10 µM. Fluorescence images were recorded at 488 nm excitation and 497–520 nm emission, using a ×20 objective, with 512 × 512 pixel resolution, and captured every 0.868 s. The data were processed with Leica Application Suite X, ImageJ and Adobe Photoshop, and traces were generated using GraphPad Prism. Dynamic fluorescence intensity values were calculated as $(F - F_0)/F_0$.

Ca^{2+} imaging and analysis with YC3.6, CGf and MatryoshCaMP6s

For Ca^{2+} imaging of the root tip using *YC3.6*, *CGf* and *MatryoshCaMP6s* transgenic seedlings, a chamber slide was made, and two strips of invisible tape were placed along the long sides of a cover slip (50 mm × 24 mm) coated with 45 µl of ½ MS medium. Each 7-day-old seedling was embedded and covered with cotton fibre, and a smaller cover slip (24 mm × 24 mm) was secured with tape. After a 10–20-min recovery, Ca^{2+} imaging was done using a Leica TCS SP8X DLS confocal microscope. Stimulus buffer (15 µl; ½ MS medium and 40 µM ABA (A100953, Aladdin) or 0.1% ethanol (mock)) was added along the edge, resulting in a final ABA concentration of 10 µM. For YC3.6, excitation was set at 458 nm, with FRET pair CFP and YFP emissions collected at 465–500 nm and 525–560 nm, respectively. Images were captured every 2.582 s at ×20 magnification with 512 × 512 pixel resolution, and fluorescence intensity was measured over root tip regions. YFP and CFP emissions of the analysed region were used for the ratio (YFP/CFP) calculation. The ratio (YFP/CFP) was calculated as $(F - F_0)/F_0$. The F value was calculated as F_{YFP}/F_{CFP}. The CGf, GCaMP6f and mCherry signals were detected with GFP (488 nm excitation, 495–520 nm emission) and mCherry (587 nm excitation, 595–635 nm emission) filters. Images were captured every 5.163 s at ×20 magnification with 512 × 512 pixel resolution. The ΔF values were calculated as $(F - F_0)/F_0$. The ratio was calculated as $\Delta(F_{GCaMP6f}/F_{mCherry})$. The MatryoshCaMP6s signals were detected with cpEGFP (488 nm excitation, 500–540 nm emission) and LSSmOrange (440 nm excitation, 570–650 nm emission) filters. Images were captured every 5.163 s at ×20 magnification with 512 × 512 pixel resolution. The ΔF values were calculated as $(F - F_0)/F_0$. The dynamic fluorescence (green/orange) was calculated as $(R - R_0)/R_0$, where R is F_{green} divided by F_{orange}. The trace was produced using GraphPad Prism.

CPKaleon fluorescence imaging in root protoplasts and data analysis

For CPKaleon fluorescence analysis with digitonin or ABA treatment, root protoplasts ($1–1.5 \times 10^5$) in 50 µl of buffer were co-transfected with 2.5 µg of *HBT–CPKaleon* and 2.5 µg of *HBT–HY5–mCherry* (control) plasmid DNA. After 10–12 h of incubation in 0.25 ml of WI buffer, the protoplasts were centrifuged at 500 *g* for 5 min. For digitonin treatment, 0.5 µl of 100 µM digitonin or H_2O (mock) was added to 1.5 µl of concentrated protoplasts in WI buffer (1 mM $CaCl_2$), giving a final concentration of 25 µM digitonin. For ABA treatment, 0.5 µl of 50 µM ABA or 0.1% ethanol (mock) was added to 2.5 µl of protoplasts in WI buffer, yielding 10 µM ABA. After 1 min, the samples were loaded onto an eight-well chamber for imaging using a Leica TCS SP8X DLS confocal microscope. CPKaleons were excited at 458 nm, with CFP and cpVenus emissions collected at 465–505 nm and 525–560 nm, respectively. HY5–mCherry excitation was set at 587 nm with 600–625 nm emission. Imaging was analysed at ×40 magnification with a 512 × 512 pixel resolution. The emissions of CFP and cpVenus in root protoplasts expressing HY5–mCherry were used to calculate the ratio (cpVenus/CFP). The ratio was calculated as $F_{cpVenus}/F_{CFP}$, with the initial mock ratio normalized to 1. Intensity data were analysed using GraphPad Prism.

Protein expression and in vitro Ca^{2+} binding assay

GCaMP6s or CRS plasmid DNA was transformed into Rosetta 2(DE3) pLysS Competent Cells (MilliporeSigma) and induced with 0.5 mM IPTG at OD_{600} = 0.6, and proteins were expressed at 18 °C for 18 h. Purification used Ni-NTA agarose beads (Qiagen), with buffer exchange in PBS via PD-10 Desalting Columns (GE Healthcare) and concentration using Amicon Ultra-0.5 Centrifugal Filters (MilliporeSigma). To determine the Ca^{2+}-dependent fluorescence intensity of CRS, 0.5 µg of purified recombinant protein was diluted in a final volume of 100 µl PBS buffer with or without 10 µM $CaCl_2$ and 1 mM EGTA. The steady-state fluorescence spectra were recorded in Corning 96-well plates (CLS3925, MilliporeSigma) using a spectramax m5 plate reader (Molecular Devices) at room temperature. The filter sets used were excitation 485 nm/emission 525 ± 15 nm for GCaMP6s and excitation 545 nm/emission 600 nm for dTomato. The fluorescence intensity values were background-subtracted using a buffer control. To analyse the Ca^{2+} binding affinity of CRS and GCaMP6s, 11 Ca^{2+} titrations were generated using a Calcium Calibration Buffer Kit #1 (Molecular Probe, Thermo Fisher Scientific) as described in the manual. The purified protein sample (0.5 µg) was added in a final volume of 100 µl Ca^{2+} titrations. The fluorescence intensity was measured as described above. K_d and Hill coefficient values were derived by fitting the fluorescence ratio (GCaMP6s/dTomato) to the Hill equation using GraphPad Prism.

RNA isolation, PCR with reverse transcription and RT–qPCR

For RNA extraction, one third of the roots were harvested using a phenol-based buffer[52] (38% phenol (Solarbio), 0.8 M guanidine thiocyanate (MilliporeSigma), 0.4 M ammonium thiocyanate (Shanghai Yuanye Bio-Technology), 0.1 M sodium acetate and 5% glycerol) at pH 5.2. PCR with reverse transcription (RT–PCR) and RT–qPCR were performed as previously described[53]. First-strand complementary DNA was synthesized from 1 µg of total RNA using the HiScript III RT SuperMix system (Vazyme) in a final volume of 20 µl. RT–PCR was conducted using a Biorad RT–PCR detection system with ChamQ Universal SYBR qPCR Master Mix (Vazyme). The primers used for RT–PCR and RT–qPCR are listed in Supplementary Table 3. The relative gene expression was normalized to the expression of *UBQ10*. Triplicate biological samples were analysed, yielding consistent results.

Cell fractionation

Approximately 40 7-day-old CRS transgenic seedlings were ground in liquid nitrogen and lysed in 1 ml of lysis buffer containing 20 mM Tris-HCl (pH 8.0), 250 mM sucrose, 25% glycerol, 20 mM KCl, 2 mM EDTA, 1% Triton X-100, 1 mM spermidine and a protease inhibitor cocktail (Complete Mini, Roche). The lysate was filtered through Miracloth (Millipore) and centrifuged at 1,000 *g* for 10 min at 4 °C. The supernatant (cytoplasmic proteins) was collected, and the pellet was washed three times. Nuclear proteins were extracted in 100 µl of nuclear lysis buffer (50 mM Tris-HCl, 10 mM EDTA, 0.5% SDS and a protease inhibitor cocktail). The proteins were separated on a 12% SDS–PAGE gel. Immunoblotting used anti-HA (Anti-HA-Peroxidase High Affinity, Roche, 1:5,000), anti-histone H3 (Histone H3 Antibody, MB9211S, Abmart, 1:5,000) and anti-tubulin (β-Tubulin Antibody for plant, M20045S, Abmart, 1:5,000) antibodies.

Imaging and defining the root cap cycle

To observe the root cap morphology changes in 5-day-old WT and *pyrpyl112458* mutant seedlings treated with or without 10 µM ABA at different time points at 3-h intervals, the seedlings were embedded in ½ MS liquid medium on a slide and then recorded using an ECHO Revolve microscope (ECHO). The microscope objective magnification was set at ×10, and images were captured every 3 h for a total of 48 h. The root cap images were collected and processed using ECHO PRO software (ECHO) and Adobe Photoshop. After each image capture, each individual seedling was carefully removed from the slide and continued to be treated in a well of a 12-well culture plate with 0.5 ml of ½ MS liquid medium containing 10 µM ABA or 0.1% ethanol (mock). A root cap cycle was defined from the initial time point (0 h) event to the next new same event[43]. To monitor the morphology changes of the complete differentiation program of the root cap in WT and *icpk* seedlings, 5-day-old WT seedlings were pretreated with 0.2 µM 3MBiP for 15 min and then treated with 10 µM ABA or 0.1% ethanol (mock). Root cap images were captured at 0 h, 24 h, 27 h, 30 h, 33 h, 36 h, 39 h, 42 h and 45 h. To monitor the root cap morphology changes of WT, *pyrpyl112458* and *snrk2.2,2.3,2.6* seedlings in response to NaCl, 5-day-old seedlings were transferred to ½ MS liquid medium containing 50 mM NaCl or H_2O (mock). Root cap cycles were captured at 0 h, 27 h, 30 h, 33 h, 36 h, 39 h, 42 h, 45 h, 48 h, 51 h, 54 h, 57 h and 60 h. The statistical and analytical basis for the root cap cycle was previously described[43]. The bar graphs of the root cap cycle were generated using GraphPad Prism.

Detection of ABA dynamics

To visualize ABA distribution in root tips, 7-day-old nlsABACUS2-400n transgenic seedlings were embedded in a chamber with 40 µl of ½ MS medium containing 200 mM NaCl or H_2O (mock) for 30 min. The dynamics of ABA signals were assessed using the ratio of FRET acceptor emission to donor emission (DxAm/DxDm) after excitation at 440 nm. Confocal Z-stack images were captured with a Leica TCS SP8X DLS confocal microscope, using a ×20 objective and 512 × 512 pixel resolution. Emission was detected at 458–482 nm for the donor (CFP) and at 520–550 nm for the acceptor (YFP). The data were processed with Leica Application Suite X and ImageJ, and the bar charts were created with GraphPad Prism.

Reporting summary

Further information on research design is available in the Nature Portfolio Reporting Summary linked to this article.

Data availability

All data underlying the findings of this study are available from the corresponding author upon request. Source data are provided with this paper.

References

1. Cheng, W. H. et al. A unique short-chain dehydrogenase/reductase in *Arabidopsis* glucose signaling and abscisic acid biosynthesis and functions. *Plant Cell* **14**, 2723–2743 (2002).
2. Cutler, S. R., Rodriguez, P. L., Finkelstein, R. R. & Abrams, S. R. Abscisic acid: emergence of a core signaling network. *Annu. Rev. Plant Biol.* **61**, 651–679 (2010).
3. Hauser, F., Li, Z., Waadt, R. & Schroeder, J. I. SnapShot: abscisic acid signaling. *Cell* **171**, 1708–1708 (2017).
4. Yoshida, T. Revisiting the basal role of ABA—roles outside of stress. *Trends Plant Sci.* **24**, 625–635 (2019).
5. Kuromori, T., Seo, M. & Shinozaki, K. ABA transport and plant water stress responses. *Trends Plant Sci.* **23**, 513–522 (2018).
6. Chen, Q. et al. Phosphorylation of SWEET sucrose transporters regulates plant root:shoot ratio under drought. *Nat. Plants* **8**, 68–77 (2022).
7. Waadt, R. et al. Plant hormone regulation of abiotic stress responses. *Nat. Rev. Mol. Cell Biol.* **23**, 680–694 (2022).
8. Luan, S. & Wang, C. Calcium signalling mechanisms across kingdoms. *Annu. Rev. Cell Dev. Biol.* **37**, 311–340 (2021).
9. Resentini, F., Ruberti, C., Grenzi, M., Bonza, M. C. & Costa, A. The signatures of organellar calcium. *Plant Physiol.* **187**, 1985–2004 (2021).
10. Liu, K. H. et al. Discovery of nitrate–CPK–NLP signalling in central nutrient–growth networks. *Nature* **545**, 311–316 (2017).
11. Edel, K. H. & Kudla, J. Integration of calcium and ABA signaling. *Curr. Opin. Plant Biol.* **33**, 83–91 (2016).

12. Albert, R. et al. A new discrete dynamic model of ABA-induced stomatal closure predicts key feedback loops. *PLoS Biol*. **15**, e2003451 (2017).
13. Konrad, K. R., Maierhofer, T. & Hedrich, R. Spatio-temporal aspects of Ca^{2+} signalling: lessons from guard cells and pollen tubes. *J. Exp. Bot*. **69**, 4195–4214 (2018).
14. Tan, Y.-Q. et al. Multiple cyclic nucleotide-gated channels function as ABA-activated Ca^{2+} channels required for ABA-induced stomatal closure in *Arabidopsis*. *Plant Cell* **35**, 239–259 (2023).
15. Boudsocq, M. & Sheen, J. CDPKs in immune and stress signaling. *Trends Plant Sci*. **18**, 30–40 (2013).
16. Scherzer, S. et al. Multiple calcium-dependent kinases modulate ABA-activated guard cell anion channels. *Mol. Plant* **5**, 1409–1412 (2012).
17. Brandt, B. et al. Calcium specificity signaling mechanisms in abscisic acid signal transduction in *Arabidopsis* guard cells. *eLife* **4**, e03599 (2015).
18. Liese, A. et al. Imaging of plant calcium-sensor kinase conformation monitors real time calcium-dependent decoding in planta. *Plant Cell* **36**, 276–297 (2024).
19. Sheen, J. Ca^{2+}-dependent protein kinases and stress signal transduction in plants. *Science* **274**, 1900–1902 (1996).
20. Choi, H. I. et al. *Arabidopsis* calcium-dependent protein kinase AtCPK32 interacts with ABF4, a transcriptional regulator of abscisic acid-responsive gene expression, and modulates its activity. *Plant Physiol*. **139**, 1750–1761 (2005).
21. Zhu, S. Y. et al. Two calcium-dependent protein kinases, CPK4 and CPK11, regulate abscisic acid signal transduction in *Arabidopsis*. *Plant Cell* **19**, 3019–3036 (2007).
22. Li, Z. et al. Abscisic acid-induced degradation of *Arabidopsis* guanine nucleotide exchange factor requires calcium-dependent protein kinases. *Proc. Natl Acad. Sci. USA* **115**, E4522–E4531 (2018).
23. Allen, G. J. et al. Cameleon calcium indicator reports cytoplasmic calcium dynamics in *Arabidopsis* guard cells. *Plant J*. **19**, 735–747 (1999).
24. Keinath, N. F. et al. Live cell imaging with r-geco1 sheds light on flg22- and chitin-induced transient $[Ca^{(2+)}]_{cyt}$ patterns in *Arabidopsis*. *Mol. Plant* **8**, 1188–1200 (2015).
25. Waadt, R., Krebs, M., Kudla, J. & Schumacher, K. Multiparameter imaging of calcium and abscisic acid and high-resolution quantitative calcium measurements using R-GECO1-mTurquoise in *Arabidopsis*. *N. Phytol*. **216**, 303–320 (2017).
26. Waadt, R. et al. Dual-reporting transcriptionally linked genetically encoded fluorescent indicators resolve the spatiotemporal coordination of cytosolic abscisic acid and second messenger dynamics in *Arabidopsis*. *Plant Cell* **32**, 2582–2601 (2020).
27. Chen, T. W. et al. Ultrasensitive fluorescent proteins for imaging neuronal activity. *Nature* **499**, 295–300 (2013).
28. Ast, C. et al. Ratiometric Matryoshka biosensors from a nested cassette of green- and orange-emitting fluorescent proteins. *Nat. Commun*. **8**, 431 (2017).
29. Li, Z., Harper, J. F., Weigand, C. & Hua, J. Resting cytosol Ca^{2+} level maintained by Ca^{2+} pumps affects environmental responses in *Arabidopsis*. *Plant Physiol*. **191**, 2534–2550 (2023).
30. Costa, A., Navazio, L. & Szabo, I. The contribution of organelles to plant intracellular calcium signalling. *J. Exp. Bot*. **69**, 4175–4193 (2018).
31. Weigand, C. et al. A ratiometric calcium reporter CGf reveals calcium dynamics both in the single cell and whole plant levels under heat stress. *Front Plant Sci*. **12**, 777975 (2021).
32. Guo, J., He, J., Dehesh, K., Cui, X. & Yang, Z. CamelliA-based simultaneous imaging of Ca^{2+} dynamics in subcellular compartments. *Plant Physiol*. **188**, 2253–2271 (2022).
33. Wu, R. et al. The 6xABRE synthetic promoter enables the spatiotemporal analysis of ABA-mediated transcriptional regulation. *Plant Physiol*. **177**, 1650–1665 (2018).
34. Rowe, J. et al. Next-generation ABACUS biosensors reveal cellular ABA dynamics driving root growth at low aerial humidity. *Nat. Plants* **9**, 1103–1115 (2023).
35. Demir, F. et al. *Arabidopsis* nanodomain-delimited ABA signaling pathway regulates the anion channel SLAH3. *Proc. Natl Acad. Sci. USA* **110**, 8296–8301 (2013).
36. Gonzalez-Guzman, M. et al. *Arabidopsis* PYR/PYL/RCAR receptors play a major role in quantitative regulation of stomatal aperture and transcriptional response to abscisic acid. *Plant Cell* **24**, 2483–2496 (2012).
37. Rodriguez, L. et al. C_2-domain abscisic acid-related proteins mediate the interaction of PYR/PYL/RCAR abscisic acid receptors with the plasma membrane and regulate abscisic acid sensitivity in *Arabidopsis*. *Plant Cell* **26**, 4802–4820 (2014).
38. Gutiérrez-Mireles, E. R. et al. An *Arabidopsis* mutant line lacking the mitochondrial calcium transport regulator MICU shows an altered metabolite profile. *Plant Signal. Behav*. **18**, 2271799 (2023).
39. Kumpf, R. P. & Nowack, M. K. The root cap: a short story of life and death. *J. Exp. Bot*. **66**, 5651–5662 (2015).
40. Bennett, T. et al. SOMBRERO, BEARSKIN1, and BEARSKIN2 regulate root cap maturation in *Arabidopsis*. *Plant Cell* **22**, 640–654 (2010).
41. Kamiya, M. et al. Control of root cap maturation and cell detachment by BEARSKIN transcription factors in *Arabidopsis*. *Development* **143**, 4063–4072 (2016).
42. Karve, R., Suárez-Román, F. & Iyer-Pascuzzi, A. S. The transcription factor NIN-LIKE PROTEIN7 controls border-like cell release. *Plant Physiol*. **171**, 2101–2111 (2016).
43. Shi, C. L. et al. The dynamics of root cap sloughing in *Arabidopsis* is regulated by peptide signalling. *Nat. Plants* **4**, 596–604 (2018).
44. Boudsocq, M., Droillard, M.-J., Regad, L. & Lauriere, C. Characterization of *Arabidopsis* calcium-dependent protein kinases: activity or not by calcium. *Biochem. J*. **447**, 291–299 (2012).
45. van Zelm, E., Zhang, Y. & Testerink, C. Salt tolerance mechanisms of plants. *Annu. Rev. Plant Biol*. **71**, 403–433 (2020).
46. Yu, B. et al. Root twisting drives halotropism via stress-induced microtubule reorientation. *Dev. Cell* **57**, 2412–2425 (2022).
47. Zhang, H. et al. ABA promotes quiescence of the quiescent centre and suppresses stem cell differentiation in the *Arabidopsis* primary root meristem. *Plant J*. **64**, 764–774 (2010).
48. Dubreuil, C., Jin, X., Grönlund, A. & Fischer, U. A local auxin gradient regulates root cap self-renewal and size homeostasis. *Curr. Biol*. **28**, 2581–2587 (2018).
49. De Rybel, B. et al. A versatile set of ligation-independent cloning vectors for functional studies in plants. *Plant Physiol*. **156**, 1292–1299 (2011).
50. Schneider, C. A., Rasband, W. S. & Eliceiri, K. W. NIH Image to ImageJ: 25 years of image analysis. *Nat. Methods* **9**, 671–675 (2012).
51. Yuan, S. et al. *Arabidopsis* cryptochrome 1 functions in nitrogen regulation of flowering. *Proc. Natl Acad. Sci. USA* **113**, 7661–7666 (2016).
52. Zepeda, B. & Verdonk, J. C. RNA extraction from plant tissue with homemade acid guanidinium thiocyanate phenol chloroform (AGPC). *Curr. Protoc*. **2**, e351 (2022).
53. Liu, K. H., McCormack, M. & Sheen, J. Targeted parallel sequencing of large genetically-defined genomic regions for identifying mutations in *Arabidopsis*. *Plant Methods* **8**, 12 (2012).

Acknowledgements

We thank A. Diener for critical reading of the paper. We thank the Horticultural Plant Biology and Metabolomics Center confocal facility at Fujian Agriculture & Forestry University and life science research core services of Northwest Agriculture & Forestry University

(NWAFU) for providing confocal microscope service, as well as Y. Wang at NWAFU for confocal microscope technical support. This research is supported by NIH grants (nos R01GM060493 and R01GM129093) to J.S. and by startup funds from NWAFU, NSFC grants (nos NSFC-32370433 and NSFC-32170270) and the Interdisciplinary Frontier Innovation Team Program of NWAFU (grant no. A1080524001) to K.-h.L.

Author contributions

Z.L., J.S. and K.-h.L. conceived and designed the project. Z.L., Y.G., R.Z., Y.L., Y.W., J.S. and K.-h.L. performed the experiments and analysed the data. Z.L., J.S. and K.-h.L. wrote the paper.

Competing interests

The authors declare no competing interests.

Additional information

Extended data is available for this paper at https://doi.org/10.1038/s41477-024-01865-y.

Supplementary information The online version contains supplementary material available at https://doi.org/10.1038/s41477-024-01865-y.

Correspondence and requests for materials should be addressed to Jen Sheen or Kun-hsiang Liu.

Peer review information *Nature Plants* thanks Sheng Luan and the other, anonymous, reviewer(s) for their contribution to the peer review of this work.

https://doi.org/10.1038/s41477-024-01865-y

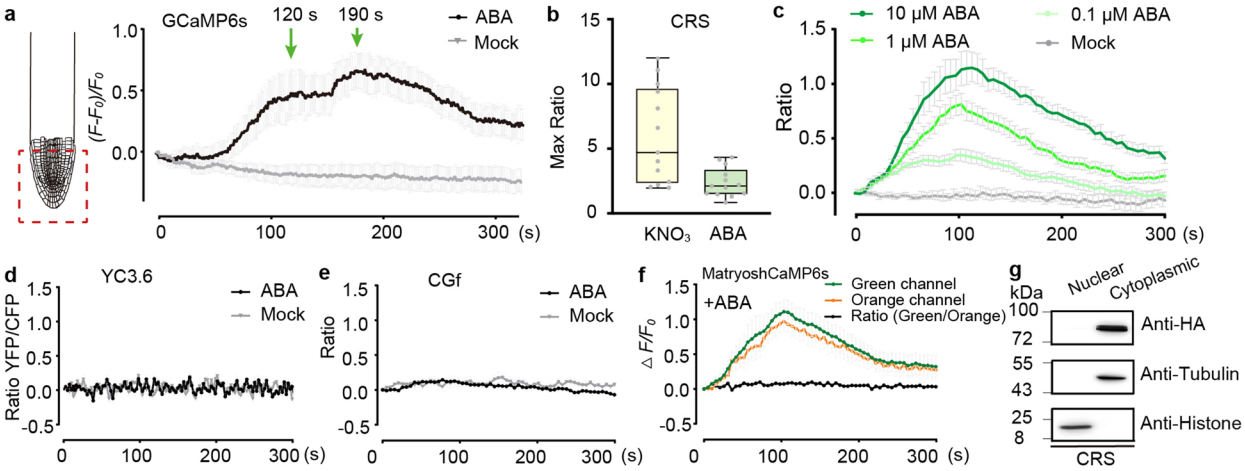

h

Name	Type	K_d (nM)	Hill coeff.	ABA -triggered [Ca^{2+}]	References
GCaMP6s	Intensiometric cpGFP (GCaMP6s)	108	2.8	+	This study, 27, 28
CRS	Ratiometric cpGFP/dTomato (GCaMP6s)	165	3.0	+	This study
MatryoshCaMP6s	Ratiometric cpGFP/LSSmOrange (GCaMP6s)	197	N/A	+	28, 30
CGf	Ratiometric cpGFP/mCherry (GCaMP6f)	203 -223	1.8 -2.1	-	31
R-GECO1	Intensiometric mApple (GECO)	482	2.1	-	24, 25, 26, 30
CamelliA_CytG	Intensiometric cpGFP (GCaMP6f)	375	2.3	-	32
YC3.6	Ratiometric CFP/cpVenus (FRET)	250	1.7	-	23, 24, 30
YCnano50	Ratiometric CFP/cpVenus (FRET)	50	2.5	-	30
Aequorin	Bioluminescence (Aequorin)	7200 -13000	N/A	-	9, 10, 30

Extended Data Fig. 1 | Detecting ABA-induced Ca^{2+} signals by different calcium biosensors. (a) Fluorescence signals of GCaMP6s stimulated by ABA in the root tip of 7-day-old plants. $(F-F_0)/F_0$ represents the relative fluorescence intensity. The red-dotted box on the left indicates the area where the Ca^{2+} signal was detected. Dual peaks (green arrow) were visible in the ABA-induced Ca^{2+} transient in the root tip at a concentration of 10 μM ABA. Error bars denote ±s.e.m., n=7 plants. (**b**) Box plot of highest fluorescence signal ratio of CRS induced by ABA or nitrate in Fig. 1e, g. Error bars denote ±s.e.m., n=13 protoplasts. Upper and lower box boundaries represent the first and third quantiles, respectively, horizontal lines mark the median and whiskers mark the highest and lowest values. (**c**) Fluorescence signals of CRS stimulated by 0.1, 1, or 10 μM ABA in the root tip of 7-day-old plants. $(F-F_0)/F_0$ represents the relative fluorescence intensity. The ratio represents the relative fluorescence ratio of GCaMP6s to dTomato, with error bars denoting ±s.e.m., n=7 plants. Fluorescence signals in the root tips of 7-day-old plants were monitored after ABA stimulation using YC3.6 (**d**), CGf (**e**), and MatryoshCaMP6s (**f**). Error bars denote ±s.e.m., data from at least three independent experiments (total number of plants: YC3.6 mock, n=7; YC3.6 ABA, n=7; CGf mock, n=10; CGf ABA, n=25; MatryoshCaMP6s (+ABA), n=6). All results were conducted in at least three biological repeats with similar outcomes. YC3.6 and CGf did not detect ABA-induced Ca^{2+} signals in root tips. MatryoshCaMP6s detected ABA-induced signals from both green (calcium signal) and orange (control) channels in root tips. ABA did not affect the green/orange ratio change in the root tips of MatryoshCaMP6s. (**g**) CRS protein localization in the Arabidopsis cytoplasm but not in the nucleus fraction. Proteins from the CRS transgenic line were analyzed by immunoblots with anti-HA, anti-Tubulin (cytoplasm marker), and anti-Histone (nucleus marker) antibodies. All experiments were conducted in at least three biological repeats with similar results. (**h**) Summary of available genetically encoded Ca^{2+} indicators used for detecting cytosolic [Ca^{2+}] of Arabidopsis plants. Hill coeff indicates Hill coefficience.

https://doi.org/10.1038/s41477-024-01865-y

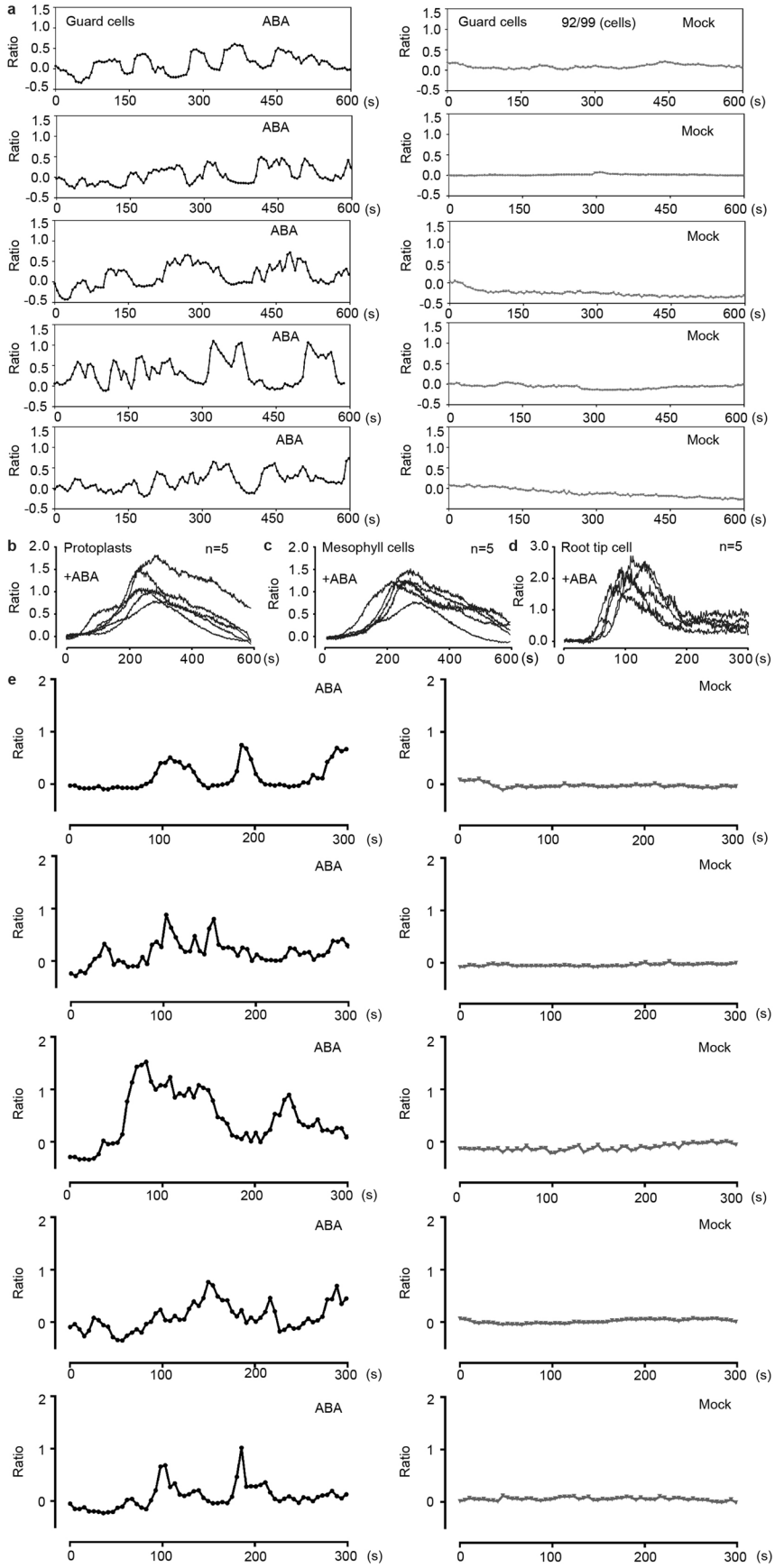

Extended Data Fig. 2 | See next page for caption.

https://doi.org/10.1038/s41477-024-01865-y

Extended Data Fig. 2 | ABA triggers Ca^{2+} transients in different cell types. Five indepedent repeats for single-cell detection of Ca^{2+} signals of CRS stimulated by ABA or mock treatment in guard cells (**a**), mesophyll protoplasts (**b**), mesophyll cells (**c**) and root tip cells (**d**). Ratio, relative fluorescence ratio of GCaMP6s to dTomato. Ca^{2+} oscillations were stimulated by ABA. We observed very few guard cells displaying different patterns of spontaneous Ca^{2+} oscillations featured with low amplitude (Ratio <0.5) and 1-2 peaks in 7 out of 99 guard cells in the mock treatment experiments. All Ca^{2+} signals were recorded at the single cell level. **e**, Five independent repeats for single-cell detection of Ca^{2+} signals of CRS-NLS stimulated by ABA or mock treatment in the nucleus of the epidermal cells in the root meristem of 7-day-old transgenic plants. Ratio, relative fluorescence ratio of GCaMP6s to dTomato. ABA, 10 μM. Left, ABA. Right, Mock.

https://doi.org/10.1038/s41477-024-01865-y

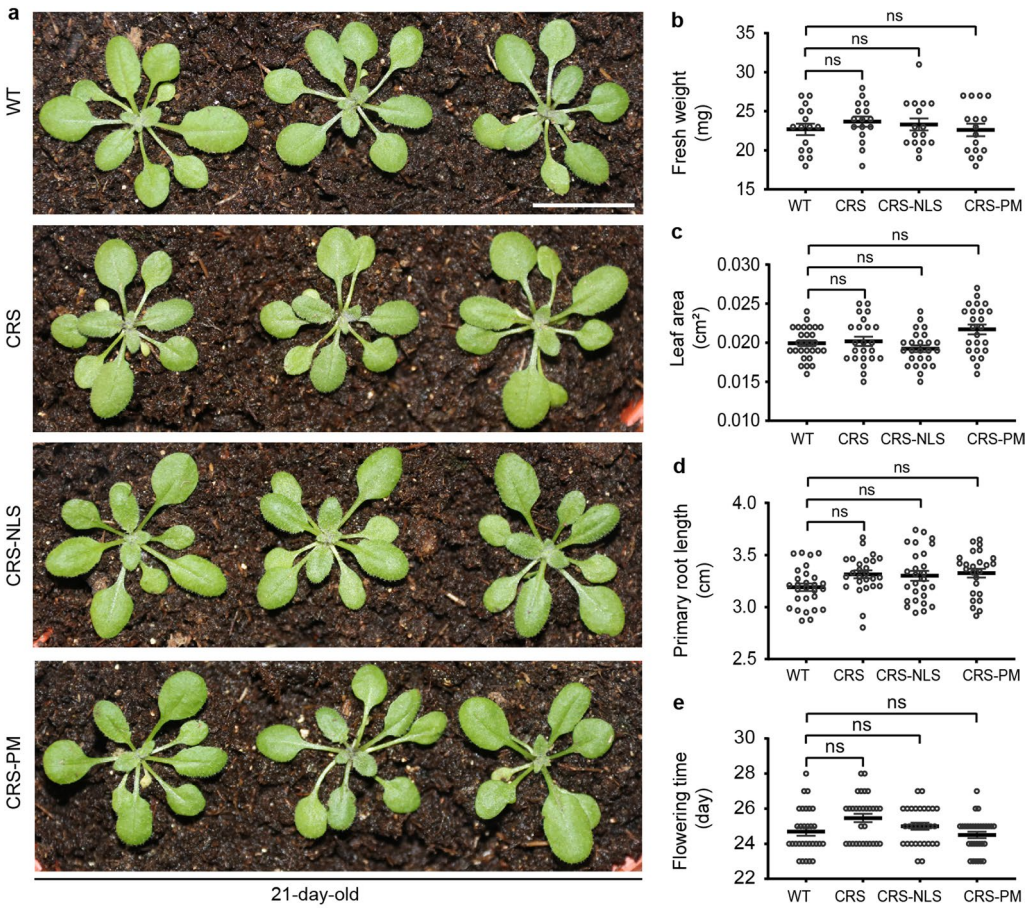

Extended Data Fig. 3 | The CRS variants do not exhibit overt growth defect phenotypes. a, WT, CRS, CRS-NLS and CRS-PM transgenic plants were grown in soil for 21 days. Scale bars, 1 cm. **b**,**c**,**d**,**e**, Resembling WT, expression of the CRS variants did not alter plant growth. Fresh weight (**b**), primary root length (**c**) and leaf area (**d**) of 7-day-old *Arabidopsis* seedlings were measured when grown on 1/2 MS solid medium. **e**, CRS, CRS-NLS, CRS-PM, and WT plants were grown in soil for statistical flowering time measurements. Error bars denote ±s.e.m., data from at least three independent experiments (total number of plants: WT, n=28; CRS, n=23; CRS-NLS, n=25; CRS-PM, n=24 (**b**), WT, n=28; CRS, n=26; CRS-NLS, n=27; CRS-PM, n=25 (**c**), WT, n=16; CRS, n=16; CRS-NLS, n=16; CRS-PM, n=16 (**d**), WT, n=30; CRS, n=30; CRS-NLS, n=30; CRS-PM, n=30 (**d**)). ns (not significant) $P > 0.05$, (statistical significance determined by two-tailed non-paired Student's *t* test). All experiments were conducted in at least three biological repeats with similar results.

https://doi.org/10.1038/s41477-024-01865-y

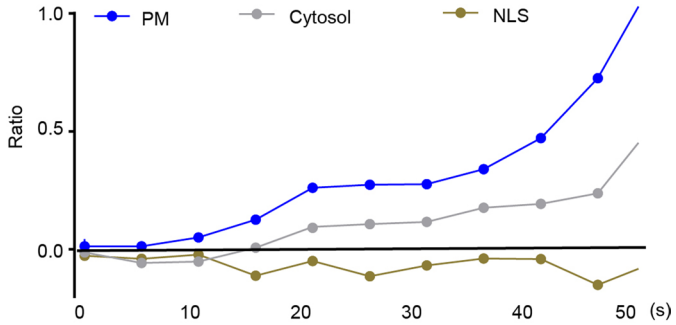

Extended Data Fig. 4 | Differential ABA-triggered subcellular Ca^{2+} dynamics within 50 s. Ca^{2+} signals of of CRS-PM, CRS, CRS-NLS within 50 s in response to ABA in the epidermal cell of the root meristem zone in 7-day-old transgenic plants. The signals were subtracted from the mock control presented in Fig. 3b–d. CRS-PM detected the ABA-induced Ca^{2+} transient first but the nuclear Ca^{2+} oscillation revealed by CRS-NLS did not start until 100 s (Fig. 3d).

https://doi.org/10.1038/s41477-024-01865-y

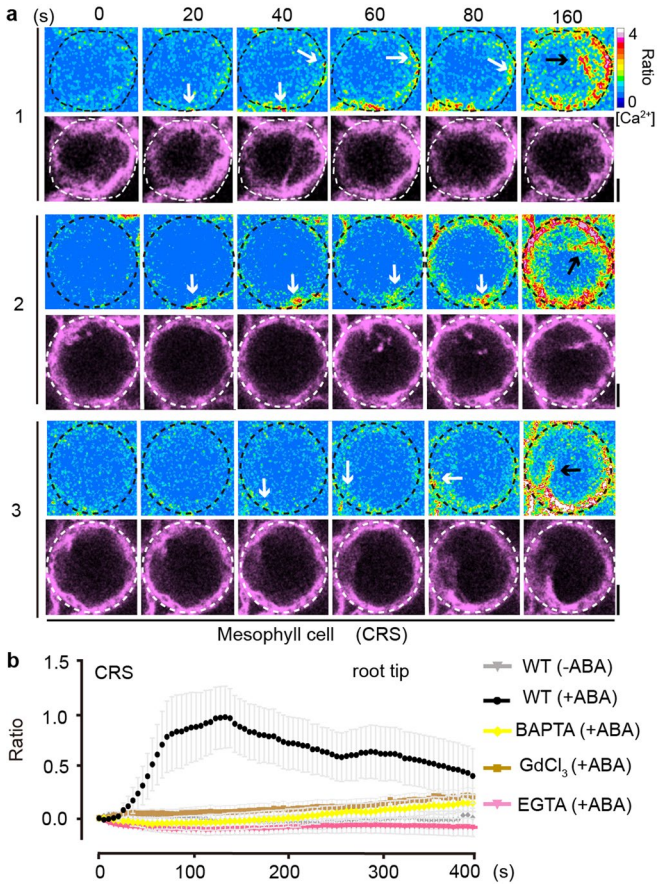

Extended Data Fig. 5 | ABA initiates a calcium signals from extracellular sources. a, Time-lapse images of ABA-induced Ca^{2+} signals near nanodomains of the plasma membrane in mesophyll cells of 7-day-old transgenic CRS plants were captured in three independent experiments. Black or white dotted circles outline the cell. White arrows indicate elevated Ca^{2+} signals. **b**, A non-selective ion channel blocker ($GdCl_3$) or Ca^{2+} chelators (BAPTA and EGTA) abolished ABA-triggered Ca^{2+} changes in Arabidopsis root tips (Extended Data Fig. 1 and Fig. 3). Error bars denote ±s.e.m., n=8 plants. Ratio, relative fluorescence ratio of GCaMP6s to dTomato. ABA, 10 µM. Scale bar, 10 µm. All experiments were conducted in at least three biological repeats with similar results.

https://doi.org/10.1038/s41477-024-01865-y

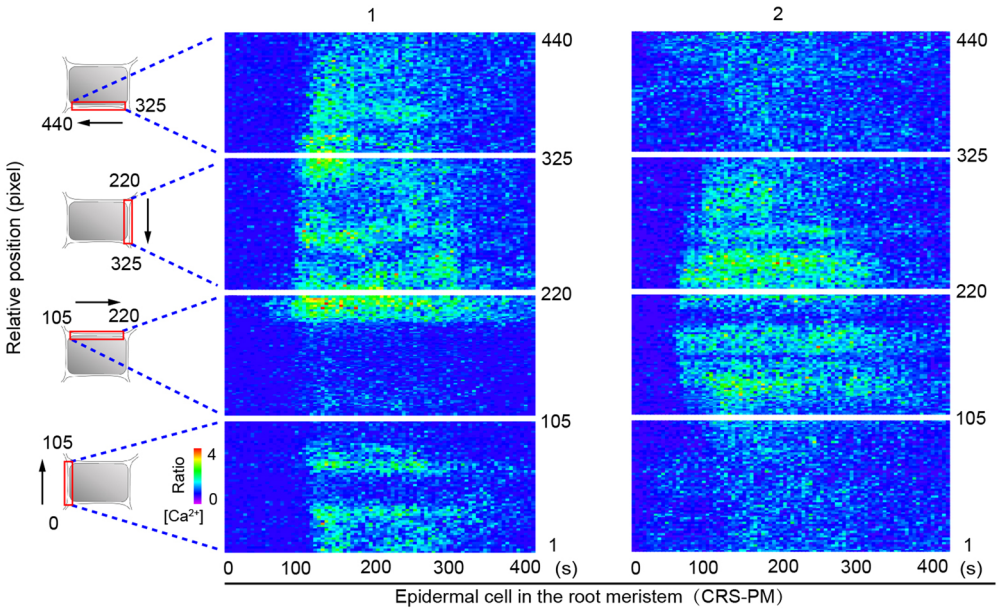

Extended Data Fig. 6 | Ca^{2+} elevation induced by ABA was not homogeneously distributed at the plasma membrane. Kymography analysis of CRS-PM in response to ABA in the epidermal cells of the root meristem zone of 7-day-old plants was performed in two more independent experiments besides the result presented in Fig. 3f. The red box indicates the detection region.

https://doi.org/10.1038/s41477-024-01865-y

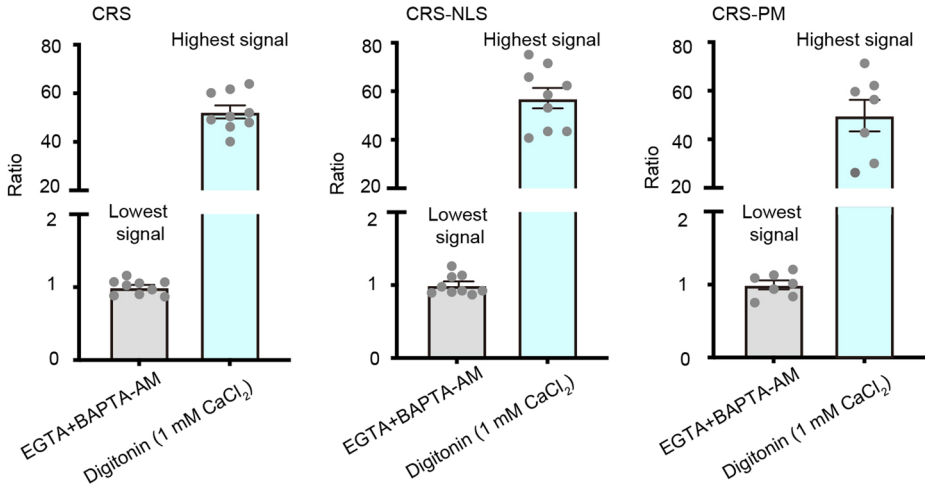

Extended Data Fig. 7 | CRS, CRS-NLS and CRS-PM show similar Ca^{2+} dynamic range in root tip cells. Range of ABA-induced changes in cytosolic [Ca^{2+}]. The highest ratio represents the maximum [Ca^{2+}] with 1mM $CaCl_2$ in digitonin-treated cells for 20 minutes [Ca^{2+}] in the root tip. The lowest ratio represents the minimum [Ca^{2+}] in the BAPTA-AM and EGTA-treated cells for 15 minutes in the root tip. Error bars denote ±s.e.m., data from at least three independent experiments (total number of plants: CRS (EGTA and BAPTA-AM), n=9; CRS (Digitonin), n=9; CRS-NLS (EGTA and BAPTA-AM), n=9; CRS (Digitonin), n=10; CRS-PM (EGTA and BAPTA-AM), n=7; CRS-PM (Digitonin), n=7). Ratio, relative fluorescence ratio of GCaMP6s to dTomato. All experiments were conducted in at least three biological repeats with similar results.

https://doi.org/10.1038/s41477-024-01865-y

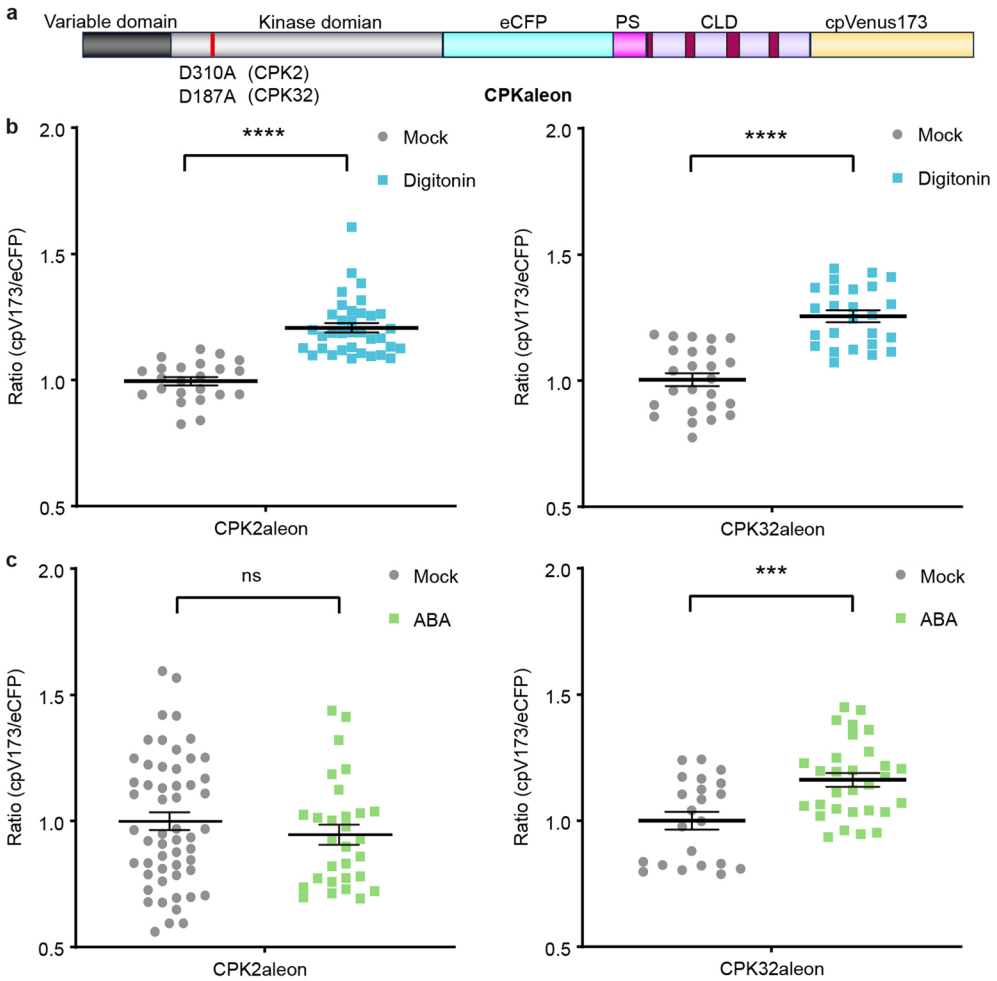

Extended Data Fig. 8 | A FRET-based sensor CPKaleon shows that CPK32aleon is activated in response to ABA in root tip protoplasts. a, Schematic diagram of CPKaleons, displaying the variable domain, kinase domain, pseudosubstrate segment (PS), and calmodulin-like domain (CLD) containing four EF-hand motifs. eGFP and cpVenus173 sandwich the CPK PS-CLD. **b**, Fluorescence accumulation in root tip protoplasts expressing CPKaleons with or without digitonin treatment. Fluorescence accumulation was quantified. Error bars denote ±s.e.m., data from at least three independent experiments (total number of protoplasts: CPK2aleon mock, n=24; CPK2aleon Digitonin, n=36; CPK32aleon mock, n=25; CPK2aleon Digitonin, n=25). ns (not significant) $P > 0.05$, **** $P < 0.0001$ (statistical significance determined by two-tailed non-paired Student's t test). **c**, CPK32, but not CPK2, is activated by ABA in root tip protoplasts. Error bars denote ±s.e.m., data from at least three independent experiments (total number of protoplasts: CPK2aleon mock, n=55; CPK2aleon ABA, n=29; CPK32aleon mock, n=23; CPK2aleon ABA, n=30). ns (not significant) $P > 0.05$, *** $P < 0.001$ (statistical significance determined by two-tailed non-paired Student's *t* test). All experiments were conducted in at least three biological repeats with similar results.

https://doi.org/10.1038/s41477-024-01865-y

a

	WT Mock			WT ABA			P value	*pyrpyl112458* Mock			*pyrpyl112458* ABA			P value
FEZ	1.086	0.861	1.053	0.253	0.304	0.333	0.0007	0.736	1.174	1.089	1.020	0.601	1.007	0.5548
SMB	0.844	1.022	1.134	0.345	0.506	0.399	0.0038	0.844	1.059	1.097	0.861	1.186	0.910	0.9164
BRN2	1.157	1.141	0.702	0.315	0.431	0.554	0.0261	1.303	0.784	0.913	0.945	0.729	1.235	0.8942
CEL5	0.952	0.961	1.087	0.349	0.400	0.201	0.0008	1.204	0.805	0.991	0.995	1.204	1.095	0.4932
XTH5	0.944	0.931	1.125	0.324	0.344	0.220	0.0007	1.109	0.873	1.019	0.857	1.052	0.773	0.3786
PE11	1.213	0.965	0.822	0.464	0.365	0.418	0.0077	1.133	0.816	1.052	0.973	0.896	1.076	0.8717
RNS3	1.114	1.009	0.877	0.344	0.414	0.574	0.0045	0.955	1.183	0.862	0.910	1.063	0.727	0.5033
MC9	1.104	0.849	1.047	0.741	0.581	0.714	0.0248	1.057	0.868	1.075	0.754	0.954	1.034	0.4642
KIN1	0.872	1.299	0.829	49.112	54.965	62.523	0.0001	1.054	1.103	0.843	1.647	1.098	1.056	0.2655

b

	WT (DMSO) Mock			WT (DMSO) ABA			P value	WT (EGTA-AM) Mock			WT (EGTA-AM) ABA			P value
FEZ	0.869	1.045	1.086	0.390	0.173	0.216	0.0014	1.070	0.879	1.058	0.610	0.516	0.425	0.0400
SMB	1.154	1.086	0.759	0.163	0.235	0.422	0.0073	0.835	0.906	0.517	0.594	0.562	0.462	0.1658
BRN2	0.958	1.098	0.945	0.448	0.378	0.415	0.0004	0.645	0.804	0.504	0.445	0.724	0.576	0.5900
CEL5	0.939	1.084	0.977	0.147	0.076	0.308	0.0005	0.672	0.730	0.900	0.404	0.602	0.459	0.0371
XTH5	1.010	1.120	0.870	0.324	0.128	0.178	0.0011	0.886	0.723	0.767	0.538	0.452	0.486	0.0054
PE11	1.226	0.877	0.897	0.471	0.144	0.279	0.0089	0.700	1.044	0.667	0.839	0.580	0.867	0.7966
RNS3	1.030	1.017	0.953	0.573	0.365	0.609	0.0037	0.755	0.633	0.759	0.696	0.694	0.440	0.3248
MC9	1.161	0.984	0.855	0.546	0.749	0.537	0.0258	0.670	0.918	0.581	0.659	0.853	0.526	0.7688
KNI1	1.001	1.098	0.902	60.242	70.845	63.617	<0.0001	1.016	1.257	1.330	49.937	47.844	51.284	<0.0001

c

	WT(+3MBiP) Mock			WT(+3MBiP) ABA			P value	*icpk* (+3MBiP) Mock			*icpk* (+3MBiP) ABA			P value
FEZ	1.199	0.869	0.932	0.296	0.381	0.288	0.0030	0.998	1.141	0.861	0.376	0.350	0.320	0.0014
SMB	0.878	0.891	1.231	0.317	0.298	0.385	0.0049	1.122	0.887	0.991	0.970	0.728	0.696	0.1402
BRN2	1.249	0.901	0.850	0.429	0.438	0.565	0.0170	0.761	0.993	1.246	0.418	0.478	0.801	0.0773
CEL5	0.865	1.094	1.041	0.305	0.192	0.203	0.0006	1.180	0.946	0.874	0.336	0.252	0.311	0.0019
XTH5	0.905	0.792	1.303	0.198	0.243	0.209	0.0073	0.801	1.026	1.172	0.234	0.248	0.175	0.0021
PE11	0.810	0.801	1.389	0.416	0.325	0.266	0.0290	0.774	1.048	1.178	0.828	0.728	1.198	0.6822
RNS3	1.101	0.792	1.107	0.554	0.611	0.405	0.0169	1.010	0.862	1.128	0.666	0.933	0.789	0.1345
MC9	0.857	1.203	0.940	0.403	0.699	0.601	0.0335	0.862	1.038	1.100	0.879	1.457	1.094	0.4775
KIN1	0.802	0.953	1.245	50.402	40.961	51.637	0.0002	0.944	0.927	1.130	27.549	33.591	34.629	0.0002

d

	WT Mock			WT NaCl			P value
FEZ	0.765	1.271	0.964	0.081	0.141	0.089	0.0038
SMB	0.989	1.071	0.94	0.281	0.291	0.226	0.0001
BRN2	0.801	1.221	0.978	0.202	0.388	0.251	0.0058
CEL5	1.012	0.855	1.133	0.242	0.238	0.161	0.0007
XTH5	1.078	0.809	1.113	0.201	0.209	0.121	0.0012
PE11	1.178	0.761	1.061	0.303	0.279	0.294	0.0047
RNS3	0.899	1.111	0.99	0.303	0.231	0.156	0.0005
MC9	1.012	0.981	1.007	0.327	0.432	0.531	0.0007
KIN1	1.322	0.881	0.797	4.111	6.332	4.377	0.0054

Extended Data Fig. 9 | Relative expression of genes associated with the root cap differentiation program in response to ABA. The analysis was conducted on 5-day-old wild-type and *pyrpyl112458* (**a**) or *icpk* (**c**) root tips in response to ABA, and 5-day-old wild-type (**b**) with or without 100 µM EGTA-AM pretreatment for 30 minutes in response to ABA. The RT-qPCR analyses of gene expression levels were normalized to the expression of *UBQ10* in each sample. The average gene expression ratio from triplicate samples was calculated and is presented in Fig. 5d, Fig. 5e and Fig. 5f. **d**, The analysis was conducted on 5-day-old wild-type root tips in response to 200 mM NaCl treatment. The RT-qPCR analyses of gene expression levels were normalized to the expression of *UBQ10* in each sample. The average gene expression ratio from triplicate samples was calculated and is presented in Fig. 6d.

https://doi.org/10.1038/s41477-024-01865-y

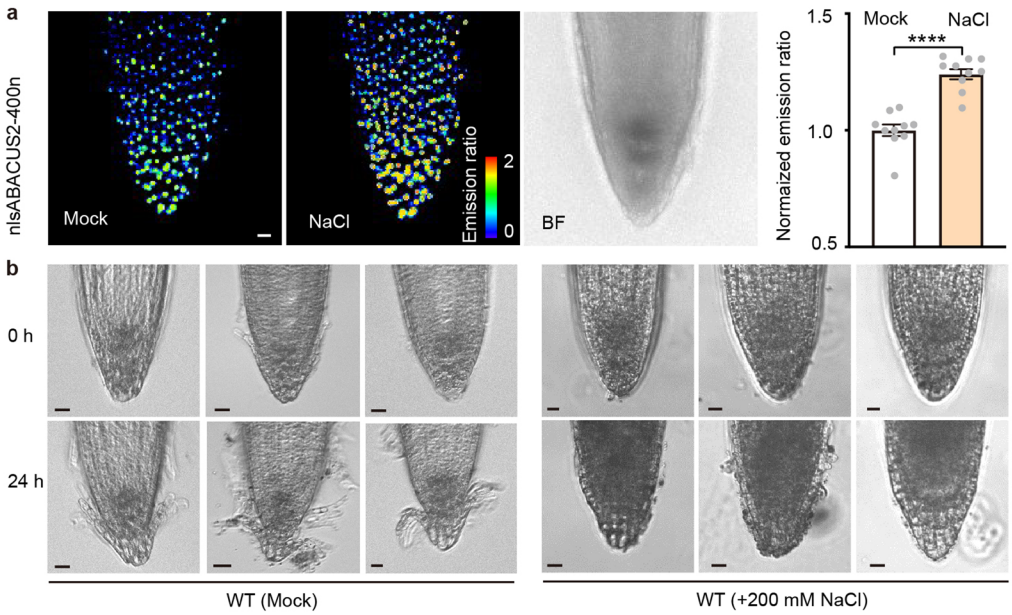

Extended Data Fig. 10 | Salt stress promotes ABA accumulation in root tips and inhibits root cap growth. a, ABA accumulation in root cap cells and epidermal cells measured using the FRET sensor nlsABACUS2-400n with or without 200 mM NaCl treatment for 30 min. Scale bars, 10 µm. ABA accumulation was quantified. Error bars denote ±s.e.m., n=10 plants. **** $P < 0.0001$ (statistical significance determined by two-tailed non-paired Student's *t* test). **b**, Treatment with 200 mM NaCl for 24 h severely inhibited root cap cycle in 5-day-old WT plants. Scale bars, 10 µm. All results are reproducible from at least three independent experiments.

nature portfolio

Corresponding author(s): Kun-hsiang Liu

Last updated by author(s): Oct 17, 2024

Reporting Summary

Nature Portfolio wishes to improve the reproducibility of the work that we publish. This form provides structure for consistency and transparency in reporting. For further information on Nature Portfolio policies, see our Editorial Policies and the Editorial Policy Checklist.

Statistics

For all statistical analyses, confirm that the following items are present in the figure legend, table legend, main text, or Methods section.

n/a	Confirmed	
☐	☒	The exact sample size (*n*) for each experimental group/condition, given as a discrete number and unit of measurement
☐	☒	A statement on whether measurements were taken from distinct samples or whether the same sample was measured repeatedly
☐	☒	The statistical test(s) used AND whether they are one- or two-sided *Only common tests should be described solely by name; describe more complex techniques in the Methods section.*
☒	☐	A description of all covariates tested
☒	☐	A description of any assumptions or corrections, such as tests of normality and adjustment for multiple comparisons
☐	☒	A full description of the statistical parameters including central tendency (e.g. means) or other basic estimates (e.g. regression coefficient) AND variation (e.g. standard deviation) or associated estimates of uncertainty (e.g. confidence intervals)
☐	☒	For null hypothesis testing, the test statistic (e.g. *F*, *t*, *r*) with confidence intervals, effect sizes, degrees of freedom and *P* value noted *Give P values as exact values whenever suitable.*
☒	☐	For Bayesian analysis, information on the choice of priors and Markov chain Monte Carlo settings
☒	☐	For hierarchical and complex designs, identification of the appropriate level for tests and full reporting of outcomes
☒	☐	Estimates of effect sizes (e.g. Cohen's *d*, Pearson's *r*), indicating how they were calculated

Our web collection on statistics for biologists contains articles on many of the points above.

Software and code

Policy information about availability of computer code

Data collection	Leica Application Suite X software (LAS X 3.1.1), Leica AF software (Leica M205 FA), a digital camera (Canon EOS 80D), ECHO PRO software, and ImageJ 1.53t (Wayne Rasband and contributors, National Institutes of Health, USA, http://imagej.nih.gov/ij, Java 1.8.0_345 (64-bit), 7057K of 3000MB (<1%)) were used in this study.
Data analysis	Microsoft Excel (Microsoft® Excel for Mac 16.89.1 (24091630)), GraphPad Prism (v.8.0), and Adobe Photoshop (v.29.0) were used for statistical analysis.

For manuscripts utilizing custom algorithms or software that are central to the research but not yet described in published literature, software must be made available to editors and reviewers. We strongly encourage code deposition in a community repository (e.g. GitHub). See the Nature Portfolio guidelines for submitting code & software for further information.

Data

Policy information about availability of data

All manuscripts must include a data availability statement. This statement should provide the following information, where applicable:

- Accession codes, unique identifiers, or web links for publicly available datasets
- A description of any restrictions on data availability
- For clinical datasets or third party data, please ensure that the statement adheres to our policy

All data underlying the findings are available from the corresponding author upon request.

Research involving human participants, their data, or biological material

Policy information about studies with human participants or human data. See also policy information about sex, gender (identity/presentation), and sexual orientation and race, ethnicity and racism.

Reporting on sex and gender	n/a
Reporting on race, ethnicity, or other socially relevant groupings	n/a
Population characteristics	n/a
Recruitment	n/a
Ethics oversight	n/a

Note that full information on the approval of the study protocol must also be provided in the manuscript.

Field-specific reporting

Please select the one below that is the best fit for your research. If you are not sure, read the appropriate sections before making your selection.

☒ Life sciences ☐ Behavioural & social sciences ☐ Ecological, evolutionary & environmental sciences

For a reference copy of the document with all sections, see nature.com/documents/nr-reporting-summary-flat.pdf

Life sciences study design

All studies must disclose on these points even when the disclosure is negative.

Sample size	The sample size used in a study is determined based on the need to have sufficient statistical power and based on previous studies in this field(Liu et al., 2017, Nature; Shi, et al., 2018, Nat. Plants). The sample size for each experiment were indicated in Figure legends.
Data exclusions	No data was excluded from the analyses.
Replication	Every experiment was subjected to at least three independent biological replicates and similar results were obtained.
Randomization	Our plant samples were randomized. To ensure uniform growth conditions, agar plates with seedlings were positioned in the growth room or chamber to maintain consistent light intensity, temperature, and humidity.
Blinding	We did not apply blinding because of the experiments were carried out by a single person and blinding is generally not used for this kind of experiments.

Reporting for specific materials, systems and methods

We require information from authors about some types of materials, experimental systems and methods used in many studies. Here, indicate whether each material, system or method listed is relevant to your study. If you are not sure if a list item applies to your research, read the appropriate section before selecting a response.

Materials & experimental systems

n/a	Involved in the study
☐	☒ Antibodies
☒	☐ Eukaryotic cell lines
☒	☐ Palaeontology and archaeology
☒	☐ Animals and other organisms
☒	☐ Clinical data
☒	☐ Dual use research of concern
☐	☒ Plants

Methods

n/a	Involved in the study
☒	☐ ChIP-seq
☒	☐ Flow cytometry
☒	☐ MRI-based neuroimaging

Antibodies

Antibodies used	anti-HA (Anti-HA-Peroxidase High Affinity, Roche-12013819001, Roche, 1:5000), anti-Histone H3 (Histone H3 Antibody, MB9211S, Abmart, 1:5000) and anti-Tubulin (βTubulin Antibody for plant, M20045S, Abmart, 1:5000) antibodies.

Validation	Information for anti-HA:(https://www.sigmaaldrich.com/US/en/product/roche/12013819001) Information for Anti-Tubuline: (https://www.ab-mart.com.cn/page.aspx?node=59&id=49688) Information for anti-Histone H3: (https://www.ab-mart.com.cn/page.aspx?node=%2077%20&id=%2031806)

Dual use research of concern

Policy information about dual use research of concern

Hazards

Could the accidental, deliberate or reckless misuse of agents or technologies generated in the work, or the application of information presented in the manuscript, pose a threat to:

No	Yes	
☒	☐	Public health
☒	☐	National security
☒	☐	Crops and/or livestock
☒	☐	Ecosystems
☒	☐	Any other significant area

Experiments of concern

Does the work involve any of these experiments of concern:

No	Yes	
☒	☐	Demonstrate how to render a vaccine ineffective
☒	☐	Confer resistance to therapeutically useful antibiotics or antiviral agents
☒	☐	Enhance the virulence of a pathogen or render a nonpathogen virulent
☒	☐	Increase transmissibility of a pathogen
☒	☐	Alter the host range of a pathogen
☒	☐	Enable evasion of diagnostic/detection modalities
☒	☐	Enable the weaponization of a biological agent or toxin
☒	☐	Any other potentially harmful combination of experiments and agents

Plants

Seed stocks	In this study, wild type (Col-0) and icpk mutant were obtained from our laboratory. The pyrpyl112458 and snrk2.2, 2.3, 2.6 seeds were provided by Dr. Jian-Kang Zhu, CGf transgenic line by Dr. Jeffrey F. Harper, YC3.6 transgenic line by Dr. Atsushi Miyawaki, nlsABACUS2-400n by Dr. Alexander Jones, and MatryoshCaMP6s from Arabidopsis biological Research Center.
Novel plant genotypes	CRS,CRS-PM,CRS-NLS transgenic plants were generated by Agrobacterium (GV3101)-mediated floral-dip method. To generate CRS-PM/CRS-NLS, CRS-PM were crossed to CRS-NLS transgenic plants. To obtain pyrpyl112458 and snrk2.2/2.3/2.6 mutants expressing CRS, pyrpyl112458 and snrk2.2/2.3/2.6 were crossed to the CRS transgenic line. In this study, we analyzed at least three independent homozygous plant lines.
Authentication	The homozygous CRS, CRS-PM, CRS-NLS, pyrpyl112458-CRS, and snrk2.2/2.3/2.6-CRS lines were characterized by genotyping, while the homozygous CRS-PM/CRS-NLS lines were identified through fluorescence microscopy.